ORGANOMETALLICS

pubs.acs.org/Organometallics Article

Chromocenium: Structural and Electronic Characterization of a Forgotten Member of the Unsubstituted Metallocenes, $[Cr(\eta^5\text{-}C_5H_5)_2]^+$

Keith A. Searles, J. Krzystek, Gayan B. Wijeratne, Patrick J. Carroll, Daniel J. Mindiola,* Timothy A. Jackson,* and Joshua Telser*

Cite This: https://doi.org/10.1021/acs.organomet.5c00396 Read Online

ACCESS | Metrics & More | Article Recommendations | Supporting Information

ABSTRACT: Simple metallocenes of the general formula $[MCp_2]^{0,+}$, where M = a wide range of 3, 4, 5d 2+ or 3+ ions and $Cp^- = \eta^5$-cyclopentadienide anion, have been known for more than half a century and are paradigms of organometallic chemistry. Chromium(III) is perhaps the most common oxidation state of chromium. Yet the corresponding metallocene, chromocenium, $[CrCp_2]^+$, has been relatively little examined, despite having been first prepared in 1962 (as an iodide salt) by E. O. Fischer who was a pioneer of metallocene chemistry. We report here the synthesis of $[CrCp_2][BAr^F]$, (BAr^F = tetrakis[(3,5-trifluoromethyl)phenyl]-borate) and its structural and spectroscopic characterization. Spectroscopic methods comprised X-band electron paramagnetic resonance (EPR) and high-frequency and -field EPR (HFEPR) in conjunction with magnetic circular dichroism (MCD). The S = 3/2 ground state of $[CrCp_2][BAr^F]$ gives spin Hamiltonian parameters: D = +4.82(1) cm^{-1}, E = 0, $g_{x(\perp)} = g_{z(\parallel)}$ = 2.00(1). The axial electronic symmetry is expected for this 5-fold symmetric complex and the positive sign of D is as found earlier for isoelectronic vanadocene, $[VCp_2]$, but the magnitude of D here is larger, qualitatively indicating the difference between isoelectronic Cr^{III} and V^{II} ions. Ligand-field theory (LFT) and quantum chemical theory (QCT) are used to analyze quantitatively the electronic structure of $[CrCp_2]^+$ on its own and in the context of its better known $3d^3$ congener $[VCp_2]$.

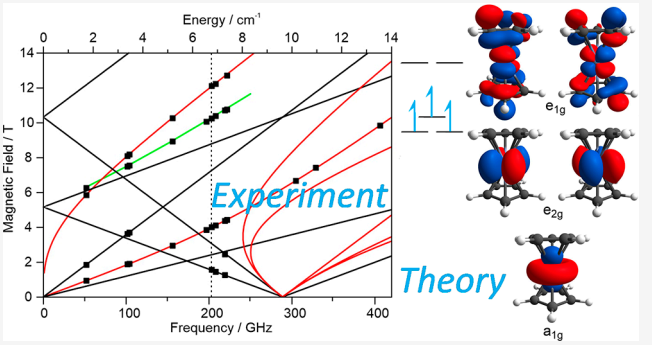

INTRODUCTION

Metallocenes, namely complexes of metal ions with cyclopentadienide anion (Cp^-) are among the most important and widely studied organometallic complexes dating back to the pioneering work of Wilkinson and Fischer.[1] Homoleptic biscyclopentadienide complexes, $[MCp_2]^{n+}$, can be neutral, such as in ferrocene (M = Fe^{II}),[2] chromocene (M = Cr^{II}),[3] or vanadocene (M = V^{II}),[4,5] but can also be cationic, such as popularized ferrocenium (M = Fe^{III})[6] or nickelocenium (M = Ni^{III}) salts.[7] Even after over 70 years since the discovery of ferrocene, new developments in fundamental metallocene chemistry are possible such as in the synthesis and characterization of a "perferrocenium", that contains Fe^{IV}[8] and the very recent report of the first structurally characterized 4d metallocene anion, interestingly with a metallocene countercation: $[Co^{III}(C_5Me_5)_2][Rh^{I}(C_5Me_5)(C_5(CF_3)_5)]$.[9]

One member of the homoleptic biscyclopentadienide series that has been given relatively short shrift is chromocenium, $[Cr^{III}Cp_2]^+$, despite its original synthesis by the metallocene pioneer E. O. Fischer early on (ca. 10 years after ferrocene).[10] The paucity of studies on $[CrCp_2]^+$ is also notable given the widespread study of Cr^{III} complexes in general[11] and the importance of organochromium species in catalysis,[12,13] in particular the oligomerization and polymerization of ethylene[14−17] as well as copolymerization reactions to make polycarbonates.[18,19] As part of our earlier experimental and computational study of $[VCp_2]$,[4,5] we realized that isoelectronic $[CrCp_2]^+$ merited a similar analysis. Moreover, as discussed below, although a few crystal structures of $[CrCp_2]^+$ with varying counteranions had been reported,[20−22] none had a "classic" weakly coordinating counteranion, of which BAr^F (tetrakis[(3,5-trifluoromethyl)phenyl]borate) is a paradigm example.[23] Having a more innocent counteranion is critical, as demonstrated by the structural distortions promoted by the anion in the case of $[FeCp_2]^{2+}$.[8] We describe here the synthesis, structural, and spectroscopic characterization of

Received: October 7, 2025
Revised: November 26, 2025
Accepted: November 28, 2025

$[CrCp_2][BAr^F]$ (**1**). The spectroscopic techniques used are conventional (X-band) electron paramagnetic resonance (EPR), its high-frequency and -field variant (HFEPR), which has been applied to related complexes,[18,24] and magnetic circular dichroism (MCD), which is a powerful technique for unraveling electronic structure,[25−30] but has been relatively less applied to early transition metal ion complexes. Using both classical ligand-field theory (LFT) and modern quantum chemical theory (QCT) ab initio computational methods, we describe the electronic structure of this hitherto somewhat neglected member of the $[M(Cp)_2]^{0,+}$ family and compare it to its neutral isoelectronic congener with V^{II}. We note that a comprehensive computational study on paramagnetic $[MCp_2]^0$ (M = V, S = 3/2; Cr, S = 1; Mn, S = 5/2; Ni, S = 1) complexes was made by Vaara and co-workers,[31] mainly in the context of calculating ^{1}H NMR spectra, but the spin Hamiltonian parameters (D, E/D, and g values) were calculated for these metallocenes along with a different Cr^{III} complex as they apparently had no relevant information on any $[CrCp_2]^+$ species.

RESULTS AND DISCUSSION

Synthesis. $[CrCp_2][BAr^F]$ (**1**) (BAr^F = tetrakis[(3,5-trifluoromethyl)phenyl]borate) was synthesized via the one-electron oxidation of $[CrCp_2]$ using $[FeCp_2][BAr^F]$.[32] An Et_2O solution of $[CrCp_2]$ was treated with $[FeCp_2][BAr^F]$ that resulted in formation of an orange solution from which **1** was obtained as an orange powder in 91% isolated yield after removal of solvent under reduced pressure and washing with pentane to remove $[FeCp_2]$. The ^{19}F NMR spectrum of **1** recorded in C_6D_6 displays a single broad resonance at −58.9 ppm ($\Delta\nu_{1/2}$ = 48.0 Hz; Figure S7). The $[CrCp_2]^+$ cation has been prepared by other, both accidental and intentional, means. The very first report of $[CrCp_2]^+$ was by Fischer and Ulm quite early in the development of metallocene chemistry.[10] They reacted a benzene solution of $[CrCp_2]$ with allyl iodide (1 equiv) producing $[CrCp_2]I$ in quantitative yield. Anion exchange with aqueous $NaBPh_4$ quantitatively yielded the discrete $[CrCp_2][BPh_4]$, the "parent" of **1**. The first report including structural characterization was by Pasynskii et al. and focused largely on $[VCp_2]$, but they also reacted $[CrCp_2]$ and $Fe_2S_2(CO)_6$, which served as carbonylation agent, producing a salt with paramagnetic $[CrCp_2]^+$ cation and diamagnetic $[CpCr^0(CO)_3]^-$ anion.[20] Subsequently, Doerrer and Green demonstrated the utility of $H_2O{\cdot}B(C_6F_5)_3$ as an oxidant of neutral metallocenes in the following reaction:

$[MCp_2] + 2H_2O{\cdot}B(C_6F_5)_3 \rightarrow [MCp_2][HOB(C_6F_5)_3{\cdots}H_2O{\cdot}B(C_6F_5)_3] + 1/2\ H_2$, where M = Cr, Fe, Co.[21] Lastly, Burin et al. studied the reaction of NdI_2 and DyI_2 with metallocenes.[22] When the reaction with DyI_2 was carried out at 80 °C, along with $[DyCp_2I]$, the complex $[Dy^{III}Cp_2I_2][Cp_2Cr^{III}]$ was formed with iododysprosocene anion and chromocenium cation.

Solid-State Structural Study of 1. Orange single crystals of **1** were obtained by layering a concentrated Et_2O solution of **1** with pentane and storing at −37 °C for 16 h. A X-ray diffraction analysis performed on a single crystal at 100 K confirmed formation of the $[CrCp_2]^+$ cation, which crystallizes in the triclinic but centrosymmetric space group $P\bar{1}$ (Figure 1). Although the asymmetric unit of **1** comprises two chromium complexes, each chromium ion resides on a crystallographic center-of-symmetry resulting in a ratio of 1:1 for the cation and anion. The Cp^- ligands of $[CrCp_2]^+$ adopt a staggered conformation in the solid-state structure. The Cr1-Cp centroid distance is 1.845(1) Å and the average of the Cr2-Cp centroid distances is 1.846(7) Å. Further information is given in Table S1 (Supporting Information).

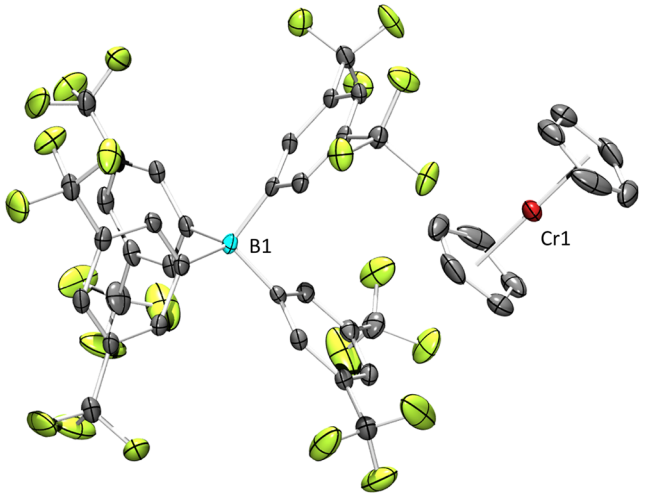

Figure 1. ORTEP drawing of the non-hydrogen atoms of $[CrCp_2][BAr^F]$ (**1**), showing selected atom labeling with ellipsoids at the 50% probability level.

Due to the volatility of neutral $[MCp_2]$, it is possible to determine their "true" (i.e., absent any packing effects) structures using gas phase electron diffraction. This method has been applied to many such complexes, the two of which that are relevant here are $[VCp_2]$ and $[CrCp_2]$. The former is isoelectronic with **1**, but with V^{II} and the latter is the neutral, Cr^{II} ($3d^4$, S = 1) parent complex. Gard et al. determined the gas phase structures of both of these complexes.[33] They favored an eclipsed (D_{5h} symmetry) structure, but could not rule out staggered (D_{5d}). The M-C bond distances are 2.280(5) and 2.169(4) Å in $[VCp_2]$, and $[CrCp_2]$, respectively. The C−C bond distances are essentially the same (1.434(3) and 1.431(2) Å, respectively). In the solid state, $[VCp_2]$ has been studied in detail by Antipin and Boese.[34] Their best results were obtained at 108 K (CSD code: CPNDYV03) and displayed a staggered conformation of the Cp^- ligands and gave a mean V−C distance of 2.269(1) Å and a mean C−C distance of 1.417 Å. In the case of $[CrCp_2]$, the sole complete structural report[35,36] was by Flower and Hitchcock who determined the crystal structure at 173 K (CSD: CYCPCR01) and found a Cr−C distance of 2.151(13) Å with a mean C−C distance of 1.401(11) Å.[37] For **1**, we find a mean Cr−C distance of 2.196(2) Å. This value is shorter than for the neutral $[VCp_2]$ also with its larger V^{II} ion, but still longer than in $[CrCp_2]$ wherein the "electron imbalance"[33] (i.e., the deviation from the "ideal" bonding situation as found in $[FeCp_2]$, namely $(e_2,a_1)^6\ e_1^0$) is smaller (3 for d^3, $(e_2,a_1)^3\ e_1^0$ and 2 for low-spin d^4, being $(e_2,a_1)^4\ e_1^0$). The average C−C distance is 1.400 Å, the same as in $[CrCp_2]$. Numerous structures have been reported for $[CrCp^*_2]^+$ (Cp^* = pentamethylcyclopentadienide anion) species as the cation in charge transfer salts, with a variety of electron acceptors, starting with the pioneering work of Miller and Epstein,[38] followed by others.[39−45] In these cases, however, not only is Cp^* markedly different from Cp as a ligand,[46] there is magnetic interaction between the $[CrCp^*_2]^+$ and the electron acceptor—the *raison d'être* of such studies, in contrast to our

https://doi.org/10.1021/acs.organomet.5c00396
Organometallics XXXX, XXX, XXX−XXX

interest in the electronic structure of isolated "plain vanilla" (i.e., $C_5H_5^-$) $[CrCp_2]^+$. We note however the complex $[CrCp^*_2][Cp^*CrCl_3]$,[47] (CSD: NAQQIF) as a representative example of an "innocent" $[CrCp^*_2]^+$ cation. In this case, the structure is staggered with a Cr−C distance of 2.193(5) Å and a Cr-Cp centroid distance of 1.83 Å.[47]

We next turn to the structures reported for $[CrCp_2]^+$ with other counteranions. In $[CrCp_2][CpCr(CO)_3]$ (CSD: FUTGIK10), the structure is eclipsed with the Cr−C distance being 2.181(5) Å and an average Cr-Cp(centroid) distance of 1.840(2) Å.[20] We see no clear reason for the eclipsed structure, although there may be weak H-bonding between the $[CrCp_2]^+$ Cp ring H atoms and the carbonyl O atoms of the anion. In the complex with $[Cp_2DyI_2]^-$ (CSD: VEBYEH), there is an almost fully eclipsed conformation of the Cp^- ligands with a Cr−C average distance of 2.197(4) Å and Cr-Cp centroid distance 1.846(2) Å.[22] In this structure there seems to be a weak H-bonding interaction of the $[CrCp_2]^+$ Cp ring H atoms to an iodide atom of the Dy-containing anion. In the complex with hydroxoborate anion (CSD: LAWROQ), there is a staggered conformation of the Cp^- ligands with a Cr−C average distance of 2.205(3) Å and the Cr-Cp centroid distance is 1.8488(14) Å.[21] In our structure, as shown in Figure S1 (Supporting Information) there is a weak π-stacking interaction between a phenyl ring of BAr^F anion and a Cp ring of the cation of interest.[48] Thus, even with BAr^F counteranion it may not be possible to have a truly "naked" $[CrCp_2]^+$ complex. With this caveat we find that spectroscopic studies of **1** are consistent whether solid state or solution forms are investigated.

Conventional EPR Spectroscopic Studies of 1. The conventional (i.e., X-band) EPR spectrum of $[CrCp_2][BAr^F]$ (**1**) is characteristic of an $S = 3/2$ species with zero-field splitting (ZFS, given by the axial parameter D and the rhombic parameter E) much larger than the microwave quantum $\left(|D| \gg \frac{\nu}{c}\right)$ and with axial symmetry ($E \approx 0$). Such a spectrum is shown in Figure 2 for **1** in toluene/thf (tetrahydrofuran) solution (1:1 v/v). The spectrum can be simulated using an effective spin, $S' = 1/2$, with $g' = [3.97, 3.97, 2.00]$ (i.e., $g'_\perp = 3.97$, $g'_\parallel = 2.00$) and nearly isotropic line widths (see Figure S2, Supporting Information). Figure 2 shows a simulation using the real $S = 3/2$ with parameters determined from HFEPR (see below). In contrast to vanadium (^{51}V, $I = 7/2$, ~100% abundance), the natural abundance of nonzero nuclear spin chromium is very low (only ^{53}Cr, $I = 3/2$, 9.5% abundance). Although satellites due to hyperfine coupling to ^{53}Cr can sometimes be observed in X-band EPR (e.g., in a formally Cr^I organometallic radical[49] and in $[Cr^I(C_6H_6)_2]I$,[50]) none was observed here for **1**, in contrast to the situation with $[VCp_2]$ for which ^{51}V hyperfine coupling was readily observed.[4,5]

The X-band EPR spectrum shown here for isolated, analytically pure **1** can be compared to that reported earlier for $[CrCp_2]^+$ found as an impurity in $[CrCp_2]$ diluted into a host lattice of diamagnetic $[MgCp_2]$.[51] This work was part of a monumental study by Ammeter on a wide variety of paramagnetic metallocenes such as $[Mn^{II}Cp_2]$, $[Fe^{III}Cp_2]^+$, $[Co^{II}Cp_2]$, and $[Ni^{III}Cp_2]^+$, all of which are Kramers (half-integer spin) systems, as are $[VCp_2]$ and $[CrCp_2]^+$. Ammeter's attempt to observe X-band EPR of $[CrCp_2]$ was apparently unsuccessful (its $S = 1$ ground state exhibits large ZFS[3] and is thus "EPR-silent" using conventional spectrometers), but an oxidation product was observed, with an unknown counter-

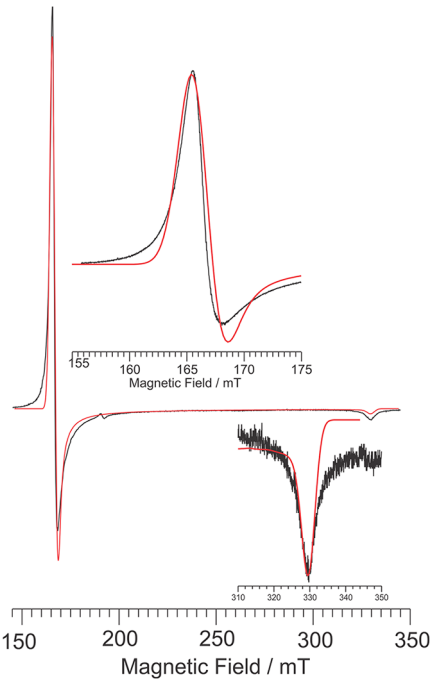

Figure 2. X-band EPR spectrum of **1** recorded in toluene/thf solution (1:1 v/v) at 77 K and 9.230 GHz (black trace). The red trace is a simulation using $S = 3/2$ with $D = +4.80$ cm^{-1} (based on HFEPR—see below), $E = 0$, $g = [1.985, 1.985, 2.000]$ and line widths (Gaussian, half-width at half-maximum (HWHM)) of 100, 80, 60 MHz. The upper inset shows an expansion of the $g_\perp$ region and the lower of the $g_\parallel$ region.

anion, in the $[MgCp_2]$ matrix. Intrinsic g values of $g_\perp = 1.977(2)$ and $g_\parallel = 2.002(2)$ were reported.[51] The $g_\perp$ value deviates slightly more from g_e than seen here, which may be a consequence of interactions with the matrix as opposed to the isolated molecules studied here, with the large and relatively noninteracting BAr^F counteranion. We also note the report of X-band EPR spectra from $[CrCp^*_2]^+$ in charge transfer salts with fullerene acceptors, with effective g' values of $g'_\perp = 3.42-3.97$, $g'_\parallel = 2.01$.[42,52] These $[CrCp_2]^+$-fullerene species clearly lack the axial symmetry expected for isolated $[CrCp^*_2]^+$, but their g' values are similar to what is seen for **1** ($g'_\perp = 3.97$, $g'_\parallel = 2.00$).

HFEPR Spectroscopy of 1. High-frequency and -field EPR (HFEPR) spectroscopy has been successfully applied in studying a variety of 3d ion systems with $S > 1/2$.[53−55] Of relevance here, besides $[VCp_2]$,[4,5] are studies on organochromium(III) complexes based on a quinoline-substituted Cp ring coordinated to a $CrCl_2$ moiety, which, as is the case here, exhibit relatively large ZFS ($D \approx 3$ cm^{-1}).[18,24]

As was the case with $[VCp_2]$, HFEPR spectra recorded for solid-state **1** were of relatively poor quality in terms of exhibiting features from individual microcrystallites. Fortunately, as was also the case with $[VCp_2]$, frozen solution HFEPR spectra of **1** gave good quality spectra with minimal baseline artifacts and decomposition/oxidation byproducts. A representative HFEPR spectrum of **1** in tetrahydrofuran (thf) solution recorded at 20 K and 208.0 GHz is shown in Figure 3. In contrast to neutral $[VCp_2]$, toluene was not a viable solvent for the ionic complex **1**, but acceptable spectra were also recorded in dichloromethane (dcm) and an additional spectrum recorded at 20 K and 104 GHz is presented in Figure S3 (Supporting Information). It is clear that the sign of

https://doi.org/10.1021/acs.organomet.5c00396
Organometallics XXXX, XXX, XXX−XXX

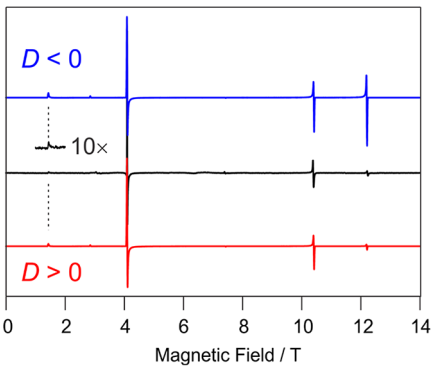

Figure 3. HFEPR spectrum of $[CrCp_2][BAr^F]$ (**1**) in toluene/thf (1:1 v/v) solution recorded at 208 GHz and 20 K (black trace). Simulations used $S = 3/2$, $|D| = 4.800$ cm^{-1}, $E = 0$, $g_{\perp(xy)} = 2.008$, $g_{\parallel(z)} = 2.000$, Gaussian line widths = 0.01 mT (HWHM). An expansion (10× intensity) of the experimental lowest field transition is shown, which is matched by the simulations. It is clear that the simulation with $D > 0$ (red trace) better matches the experimental intensities than that with $D < 0$ (blue trace).

D is positive, namely that the $m_S = \pm 1/2$ doublet is lower in energy, which agrees with the X-band results, and with the finding for $[VCp_2]$. Figure 4 presents a 2D map of turning

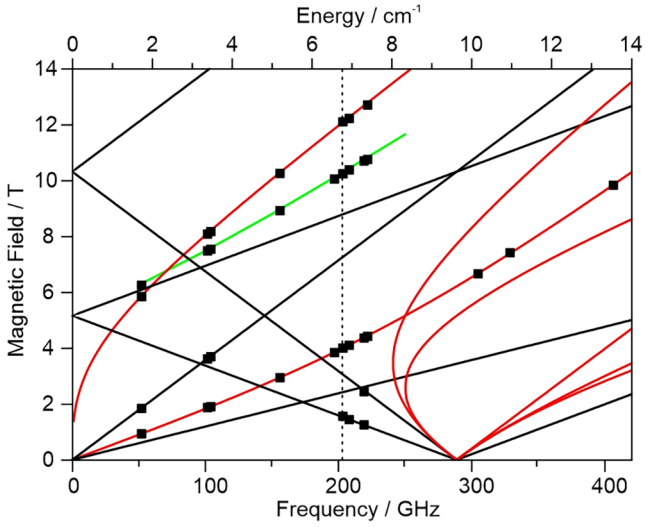

Figure 4. Field versus frequency (energy) map of turning points in **1**. The best-fit $S = 3/2$ spin Hamiltonian parameters are $|D| = 4.815(5)$ cm^{-1}, $E = 0.0003(3)$ cm^{-1}, $g_{x(\perp)} = 2.004(2)$, $g_{z(\parallel)} = 2.012(7)$. Red lines are $B_0 \| x$ (= y; $\perp$ direction) and black lines are $B_0 \| z$ ($\parallel$ direction). The green line is an off-axis turning point. The dashed vertical line represents the frequency at which the spectrum shown in Figure 3 was recorded.

points in the powder spectra versus multiple microwave frequencies with calculated lines. This type of presentation has been widely used for HFEPR data[53] and shows here the accuracy and precision of the $S = 3/2$ spin Hamiltonian least-squares fit to the entire data set, namely $D = 4.815(5)$ cm^{-1}, $E = 0.0003(3)$ cm^{-1}, $g_{x(\perp)} = 2.004(2)$, $g_{z(\parallel)} = 2.012(7)$. Given the experimental precision, a more realistic set of $S = 3/2$ spin Hamiltonian parameters is $D = +4.82(1)$ cm^{-1}, $E = 0.00$, $g_{x(\perp)} = g_{z(\parallel)} = 2.00(1)$. For comparison, $[VCp_2]$ gave $D = +2.836(2)$ cm^{-1}, $g_\perp = 1.991(2)$, $g_\parallel = 2.001(2)$.[5]

The g-values, being essentially the free electron value, are uninformative as to electronic structure; however, the ZFS is informative. Qualitatively, two points can be noted here. First, as was the case for $[VCp_2]$, **1** has rigorously axial electronic symmetry as expected from its crystal structure. Second, the positive sign of D is the same as for $[VCp_2]$, but is larger in magnitude (by ∼70%), which can be the consequence both of greater spin−orbit coupling (SOC) in Cr^{III} versus V^{II} and potentially the stronger bonding interactions for a 3+ versus 2+ ion. Ligand-field theory (LFT) and quantum chemical theory (QCT) calculations will address these points quantitatively below.

MCD Spectroscopy. The low-temperature magnetic circular dichroism (MCD) spectrum of a mull sample of **1** shows a rich collection of temperature-dependent C-terms (Figure S4)[56] from 15 000−28 500 cm^{-1} (Figure 5, top).[25] At

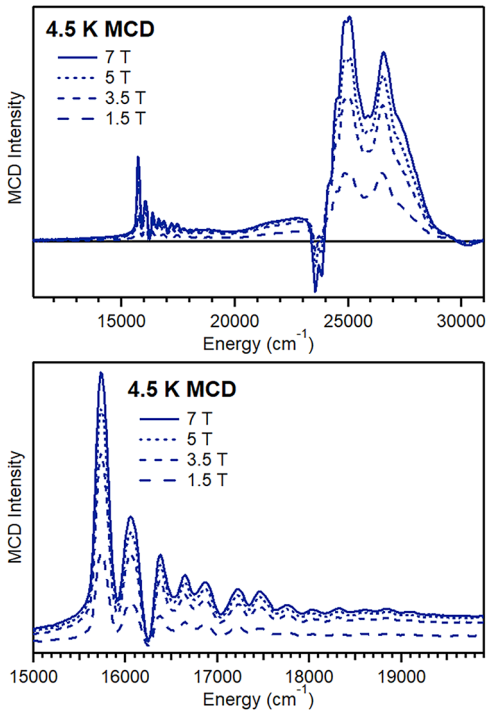

Figure 5. Top: Variable-field, 4.5 K MCD spectra of a mull sample of $[CrCp_2][BAr^F]$ (**1**). Bottom: Expanded view of the vibronic structure in the variable-field, 4.5 K MCD spectra of a mull sample of **1**.

lower-energy, the MCD spectrum contains a progression of at least 12 sharp features, beginning at 15 500 cm^{-1} and stretching to 19 000 cm^{-1} (Figure 5, bottom). The higher-energy region of the spectrum (23 000−29 000 cm^{-1}) contains the most intense MCD features, including positive bands at 24 950 and 26 600 cm^{-1} and a negative feature near 23 500 cm^{-1}. Some fine structure is observed for the bands at 23 500 and 24 950 cm^{-1}. The band energies and amplitudes are given in Table S2 (Supporting Information). The positions of these features correspond well to previously reported electronic absorption bands of $[CrCp_2]^+$ (17 860, 21 980, and 27 030 cm^{-1}).[57]

The low-energy MCD feature of **1**, which consists of a series of closely spaced bands (Figure 5, bottom), is attributed to a set of Franck−Condon vibronic progressions. In a vibronic profession, the individual MCD features arise from excitations to different vibrational sublevels of an electronic excited state.

https://doi.org/10.1021/acs.organomet.5c00396
Organometallics XXXX, XXX, XXX−XXX

Such progressions are often simulated under a harmonic approximation by using the following Poisson distribution

$$\Delta\varepsilon = \sum_n \Delta\varepsilon_{0\to 0}\frac{S^n}{n!}e^{[-(2.733/(\mathrm{FWHM})^2)(E-n\Delta E-E_{0\to 0})^2]} \quad (1)$$

where $\Delta\varepsilon_{0\to 0}$ and $E_{0\to 0}$ are respectively the intensity and energy of the first vibronic transition (*i.e.*, the first peak in the progression), S is the Huang–Rhys factor that reflects the width and displacement of the excited-state potential energy surface relative to the ground state, E is the photon energy, ΔE is the vibrational spacing, and fwhm is the full-width at half-maximum of each vibronic band.[27−30]

An analysis of the positions of the band maxima shows an irregular spacing, with the band-to-band separation varying from 240 to 356 cm^{-1}. This spacing, as well as an unusual intensity distribution, indicate that this progression contains contributions from more than one excited state. In support, attempts to simulate this progression as a standard Poisson distribution describing a single excited state (see eq 1) led to very poor fits. A minimum of three separate excited states, each with its own Franck–Condon vibronic progression, was required to obtain even modest agreement between experiment and theory over a limited energy range (Figure S5, top). In these simulations, common bandwidths (fwhm) were assumed for each excited state, Huang–Rhys factors (S) were varied slightly for each excited state, while the electronic excited-state origins ($E_{0\to 0}$) and MCD intensities ($\Delta\varepsilon_{0\to 0}$) were varied parameters. A very crude fit, however, was also obtained using an EPR simulation program (DDPOWH by J. Telser) that gives a semiquantitative picture of the vibronic coupling. This "Ansatz" procedure is described in Supporting Information and shown in Figure S6.

A possible origin of this vibronic coupling can be gleaned from vibrational (IR and Raman) studies on $[MCp_2]$ complexes by Aleksanyan et al.,[58,59] including $[VCp_2]$ and $[CrCp_2]$. For these two complexes as solids at 90 K there are low frequency Raman active bands as follows:[58] $\nu_{22}(E_{2u}$ in D_{5d}, which is a Cp-M-Cp bend[60]) at 183 cm^{-1} (M = V, weak; not seen for M = Cr), $\nu_4(A_{1g}$, which is a Cp-M symmetric stretch[60,61]$)$[62] at 258 cm^{-1} (M = V, medium), 273 cm^{-1} (M = Cr, strong) and $\nu_{16}(E_{1g}$, which is a ring tilt[60,61]) at 331 cm^{-1} (M = V, medium), 370 cm^{-1} (M = Cr, very weak). Equally relevant is an IR active band $\nu_{11}(A_{2u}$, which is a Cp-M asymmetric stretch[60,61]) at 380 cm^{-1} (M = V, strong intensity), 408 cm^{-1} (M = Cr, medium). We have no explanation as to why vibronic coupling was not observed previously in vanadocene,[5] and purely vibrational studies on **1** would be complicated by the BAr^F counteranion, so we do not know the exact energies of ν_4 and ν_{11} or other possibly relevant modes such as ν_{16} or ν_{21}. Nevertheless, it appears that in $[CrCp_2]^+$ there is vibronic coupling observed between electronic transition(s) and Cp-M stretches as well as possibly other low energy modes involving the metal ion.

While the low-energy region of the MCD spectrum of **1** required the inclusion of vibronic effects, the higher-energy region (22 000−28 500 cm^{-1}) could be analyzed in a more conventional fashion,[63,64] with each electronic transition approximated by a broad, Gaussian function (Figure S5, bottom). This analysis revealed the presence of at least five electronic transitions. Two of these bands (bands 2 and 3) appear to form a pseudo-*A* term, which are two oppositely signed and energetically adjacent MCD bands that give rise to a derivative-shaped feature.[25] Both components of this pseudo-*A* term show fine structure, with sharp features observed from 23 557−25 907 cm^{-1}. These features are spaced at irregular intervals, ranging from 234 to 355 cm^{-1}, but the average energy spacing is close to that observed for the Franck–Condon progression at lower energy. Because of this similarity in energy spacing, we attribute the fine structure on bands 2 and 3 to a Franck–Condon vibronic progression. Because the progression is coincident with bands 2 and 3, a detailed simulation was not performed. The remaining three MCD bands (bands 1, 4, and 5) are positively signed and show no vibronic structure.

Following our analysis of the optical properties of the isoelectronic $[VCp_2]$,[5] we expect three spin-allowed ligand-field transitions for $[CrCp_2]^+$: $^4A_{2g} \to {}^4E_{1g}(I)$, $^4A_{2g} \to {}^4E_{2g}$, and $^4A_{2g} \to {}^4E_{1g}(II)$, using symmetry labels from the D_{5d} point group. Each excited state arises from a one-electron excitation relative to the $^4A_{2g}$ $(a_{1g})^1(e_{2g})^2(e_{1g})^0$ configuration, as summarized in Table 1. Because each excited state is orbitally degenerate, under ideal conditions, each should appear as a pseudo-*A* term in the MCD spectrum of $[CrCp_2]^+$. However, overlap of the bands can lead to cancelation of the positive and negative components, complicating spectral interpretation. This appears to be the case for $[CrCp_2]^+$, where only one pseudo-*A* term (bands 2 and 3) is apparent. Given this complication, we developed assignments of the MCD features using electronic structure computations, as described below.

Table 1. States and Configurations for Quartet Terms of $[CrCp_2]^+$

state	configuration	excitation relative to ground state	approximate energies from MCD data (cm^{-1})
$^4A_{2g}$	$(e_{2g})^2(a_{1g})^1(e_{1g})^0$	NA[a]	
$^4E_{1g}(I)$[b]	$(e_{2g})^2(a_{1g})^0(e_{1g})^1$	$a_{1g} \to e_{1g}$[c]	23 600
$^4E_{2g}$	$(e_{2g})^1(a_{1g})^1(e_{1g})^1$	$e_{2g} \to e_{1g}$	25 000
$^4E_{1g}(II)$[b]	$(e_{2g})^1(a_{1g})^1(e_{1g})^1$	$e_{2g} \to e_{1g}$	28 000

[a]Not applicable. [b]The $^4E_{1g}$ (I) state arises from free-ion term ^4F and the $^4E_{1g}$ (II) state arises from free-ion term ^4P. [c]The e_{2g} orbital corresponds to $d_{xy}, d_{x^2-y^2}$ and the e_{1g} orbital corresponds to d_{xz}, d_{yz}.

ELECTRONIC STRUCTURE COMPUTATIONS FOR $[CRCP_2]^+$[65]

Ligand-Field Theory (LFT) Calculations. *Electronic Transitions.* The application of LFT to the $3d^3$ metallocene complexes $[VCp_2]$ and $[CrCp_2]^+$ was pioneered by Pavlík and co-workers,[57] They reported a synthetic procedure only for $[VCp_2]$ and its spectra in *n*-pentane and Et_2O were presented, but it is unclear from their paper whether they recorded any electronic absorption spectra themselves for the Cr^{III} complexes (the biscarborane complex $[Cr(1,7\text{-}B_9C_2H_{11})_2]^-$ and mixed carborane-metallocene complex $[CrCp(1,7\text{-}B_9C_2H_{11})]$ were also studied). Nevertheless, they reported bands at 560 nm (17 860 cm^{-1}; ε = 270 L mol^{-1} cm^{-1}), 455 nm (21 980 cm^{-1}; ε = 210 L mol^{-1} cm^{-1}), and 370 nm (27 030 cm^{-1}; ε = 630 L mol^{-1} cm^{-1}). These were assigned to the three transitions given in Table 1: $^4A_{2g} \to {}^4E_{1g}(I)$, $^4A_{2g} \to {}^4E_{2g}$, and $^4A_{2g} \to {}^4E_{1g}(II)$, respectively. They employed the classical crystal-field parameters of Ballhausen,[66] as also done by Warren,[67] to quantify the bonding. We have reproduced their results, in which the bands are fitted exactly using (in

https://doi.org/10.1021/acs.organomet.5c00396
Organometallics XXXX, XXX, XXX−XXX

cm^{-1}): Dq = 0 (since this is a purely axial system, with no cubic crystal-field interaction), Ds = −4299.7 (our phase definition is opposite to that used by Pavlík[57] who had Ds = +4299), Dt = 2087, and Racah B = 513 (55% of the free-ion value;[68] Racah C is set large for fitting purposes; use of free-ion C/B = 3.97[69] gives C = 2040). The resulting energy levels are given in Table S3 (Supporting Information). The larger (magnitude) Ds parameter for **1** versus $[VCp_2]$ indicates stronger bonding in the 3+ versus 2+ ion complex.

Our optical spectra, however, support a different assignment, namely that the band near 17 000 cm^{-1} is likely from a doublet excited state, and the three spin-allowed bands (in cm^{-1}) are closely spaced at: 23 500 ($^4A_{2g} \rightarrow {}^4E_{1g}$(I)), 25 000 ($^4A_{2g} \rightarrow {}^4E_{2g}$), and 28 000 ($^4A_{2g} \rightarrow {}^4E_{1g}$(II)). In this case, perhaps because the lines are closely spaced, the fit can go awry (e.g., drive B to a very low value), but with care it is possible to fit the three bands exactly using the following parameters (in cm^{-1}): Ds = −4216, Dt = 2714, and B = 253 (only 27% of the free-ion value,[68] so that the free-ion C/B gives C = 1005). These crystal-field (bonding) parameters are close to those reported earlier.[57] The low B value is peculiar and the correspondingly low value for C gives very low-lying doublet excited states with none near ∼17 000 cm^{-1}. We therefore included another band for the fitting, namely a doublet at this energy. The fit was repeated allowing C to vary within a reasonable range. This procedure allowed the nominally spin-forbidden band to be matched exactly. Allowing Ds, Dt, B, and C all to vary within narrow ranges led to deviations between experiment and calculation of <1 cm^{-1}, far better than the experimental precision. The final fit parameters were (in cm^{-1}): Ds = −4215.77, Dt = 2713.89, B = 252.975, and C = 2626.86 (71% of the free-ion value). It is less common, but not impossible that the Racah B and C parameters diverge differently from their free-ion values.[70,71] The resulting energy levels are given in Table S4 (Supporting Information). Lastly, we note that even the earlier band assignments[57] give a doublet excited state calculated at ∼19 000 cm^{-1} (Table S3) roughly in the range proposed by our optical spectroscopy.

Spin Hamiltonian Parameters. A final application of classical LFT is to calculate the S = 3/2 spin Hamiltonian parameters for $[CrCp_2]^+$. To do so, we include spin−orbit coupling (SOC) parametrized by the single-electron SOC constant, ζ = 274 cm^{-1} for free-ion Cr^{3+} (ζ = 169 cm^{-1}, for free-ion V^{2+}).[68] Reducing ζ from the free-ion value to 210 cm^{-1} (77% of the free-ion value, similar to the reduction for C), gives a zero-field splitting between the $m_S = \pm 1/2$ ground state spin doublet and the $m_S = \pm 3/2$ (i.e., $D > 0$) of 9.467 cm^{-1}; since the system is axial, D = 9.467/2 = +4.734 cm^{-1}. This D value is from only SOC (D_{SOC}); spin−spin coupling (SSC)[72] is not included. As described below in the QCT section the SSC contribution (D_{SSC}) could be as great as one-third of the total ZFS. In this case, e.g., ζ = 180 cm^{-1} (66% of the free ion value) gives D_{SOC} = +3.38 cm^{-1}, which might be sufficient when combined with D_{SSC}. In any case, the agreement is quite good given the simple model used. Addition of an external magnetic field (B_0 = 350 mT, typical for X-band EPR) for either ζ value gives $g'_\perp$ = 3.94, $g'_\parallel$ = 2.00, which agrees remarkably well with the X-band data: $g'_\perp$ = 3.97, $g'_\parallel$ = 2.00.

Angular Overlap Model (AOM) Analysis. An alternate LFT method is to use the angular overlap model (AOM),[73−75] which we have used for "traditional" complexes with coordination numbers of three,[76] four,[77] five,[78] and six,[79] but did not do so in our study on $[VCp_2]$.[5] We have now applied the AOM to $[CrCp_2]^+$, and by extension, could do so to any D_{5d} (or D_{5h}) metallocene. The present crystal structure of **1** affords the angle from a ring C to the Cp ring centroid to the Cr^{III} ion of 32.85(40)°. Essentially the same value, 33.0(5)°, obtains for the other relevant structures (CSD codes: LAWROQ,[21] FUTGIK,[20] and VEBYEH[22]). We therefore define for D_{5d} symmetry five C ligands at θ = 33° and another five at θ = 147°, with $\phi_{1-5} = [72(n-1)]°$ and $\phi_{6-10} = [36 + 72(n-1)]°$, where n = 1−5 (for D_{5h}, which we did not use, $\phi_{6-10} = \phi_{1-5}$). The absorption bands including a spin-forbidden transition at 17 000 cm^{-1} were fitted following the same procedure as above. The spin-allowed bands were first fitted to provide Racah B (and the bonding parameters), and then the spin-forbidden transition was included to provide C. All ten Cp carbon donors were held identical and both types of π-bonding (π-s(y) and π-c(x))[73,74] were included, but it was found that only π-s was needed for successful fitting. As shown in Table S5, in the MCp_2 geometry this type of π-bonding particularly affects the energy of the d_{xz},d_{yz} orbitals (e_1) while π-c affects primarily the d_{z^2} orbital (a_1) energy. The resulting fit parameters (all in cm^{-1}) were: ε_σ(C) = 4484.41, $\varepsilon_{\pi-s}$(C) = 6505.77, $\varepsilon_{\pi-c}$(C) = 0; B = 279.17, C = 2553.68. The calculated energy levels are given in Table S6 and were very close to those obtained from the crystal-field model (see above) although the slightly larger B value is more reassuring, now being 30% of the free-ion value; the C value, determined from fitting, is 70% of its free-ion value.[68] Addition of SOC (ζ = 180 cm^{-1}) and an external magnetic field gave spin Hamiltonian parameters essentially identical to those obtained from the crystal-field model and thus in good agreement with experiment. For comparison with QCT calculations (see below) the calculated electronic transitions including SOC are given in Table 2 and match the observed bands reasonably well. The AOM parameters give single electron d orbital relative energies of d_{xy},$d_{x^2-y^2}$ (e_{2g}) at 0, d_{z^2} (a_{1g}) at 2687 cm^{-1} (0.333 eV), and d_{xz},d_{yz}(e_{1g}) at 27 785 cm^{-1} (3.197 eV). These values should not be taken too literally, but suggest that in $[CrCp_2]^+$ the d_{z^2} orbital is relatively low lying in energy (i.e., close to the d_{xy},$d_{x^2-y^2}$ orbitals), which is in agreement with the quantum chemical theory described in the following section.

For completeness, we also applied the same AOM fitting procedure to $[VCp_2]$ using the absorption bands we reported earlier.[5] In this case the relevant angle is 32.08(2)° using the structure obtained at 108 K.[34] The resulting fit parameters (all in cm^{-1}) were: ε_σ(C) = 3877.5, $\varepsilon_{\pi-s}$(C) = 4795.5, $\varepsilon_{\pi-c}$(C) = 0; B = 454.22, C = 1882.26. These Racah parameters are respectively ∼60 and ∼65% of the free-ion values for V^{2+},[69] which is quite reasonable. Qualitatively, it can be seen that the bonding parameters, both ε_σ and ε_π, are smaller for vanadocene, particularly the π-bonding which is much stronger for $[CrCp_2]^+$. The calculated energy levels are given in Table S7. These AOM parameters give d_{z^2} at 4953 cm^{-1} (0.614 eV) and d_{xz},d_{yz} at 21 062 cm^{-1} (2.61 eV), so that the essentially π^* e_{1g} orbitals are lower in energy than in $[CrCp_2]^+$. Inclusion of SOC with ζ = 120 cm^{-1} (∼70% of the free-ion value[68]) gives D_{SOC} = +2.01 cm^{-1}, close to the observed value (D = +2.836(2) cm^{-1}), which includes D_{SSC}.

Quantum Chemical Theory (QCT) Calculations. *Molecular Structures.* In considering the electronic structure of $[CrCp_2]^+$ we focused on two models. One model employed the crystal structure coordinates from the X-ray structure reported in this work, with the positions of the hydrogen atoms

https://doi.org/10.1021/acs.organomet.5c00396
Organometallics XXXX, XXX, XXX−XXX

Table 2. Zero-Field Splitting (ZFS) Parameters and Ligand-Field Energies (all in cm^{-1}) for $[CrCp_2]^+$ from DFT, CASSCF/NEVPT2, and LFT/AOM Calculations

		XRD 1			
	experiment[a]	DFT	CAS(7,7)/NEVPT2	SORCI	AOM[c]
D	+4.82	3.34	4.74	5.21	3.54
E/D	0	0	0	0	0
D_{SSC}		1.19	1.01	0.81	
E/D_{SSC}		0	0	0	
D_{SOC}		2.15	3.73	4.40	3.54
E/D_{SOC}		0	0	0	0
$^4A_{2g}$		0	0	0	0
$^2E_{1g}$			14 040	13 497	8826
			14 040	13 727	10 450
$^2E_{1g}$	15 800		16 586	15 887	17 007
	15 900		16 587	15 893	17 012
$^2A_{1g}$	16 500		17 431	15 411	13 166
$^2A_{2g}$			18 678	17 654	10 967
$^4E_{1g}$(I)	23 500	25 042	25 001	23 090	23 447
	23 710	25 152	25 003	23 116	23 567
$^2E_{1g}$			27 305	24 562	24 741
			27 307	24 601	24 917
$^4E_{2g}$	25 000[b]	25 269	26 903	24 966	25 097
		25 673	26 903	24 966	25 280
$^4E_{1g}$(II)	28 000[b]	28 269	31 060	28 388	27 946
		28 592	31 063	28 399	28 067

[a]Zero-field splitting parameters from HFEPR experiments and electronic transition energies from MCD experiments. [b]Because we do not observe pseudo-*A* term for these states, the assignment of the components of these excited states are unclear. Nonetheless, the cluster of MCD features from 25 000 to 30 000 cm^{-1} is attributed to these excited states. [c]AOM parameters given in Table S6 with the addition of SOC using ζ = 180 cm^{-1}.

optimized using DFT methods. The refinement of the hydrogen-atom positions using DFT was employed because the positions of these atoms are not as well-defined as those of heavy atoms in the experimental structure. The second model of $[CrCp_2]^+$ was generated using DFT geometry optimizations for the staggered (D_{5d}) structure, with the positions of all atoms subject to optimization. These calculations imposed C_{2h} symmetry constraints, as the higher-symmetry D_{5d} point group is not available in *ORCA*. We focused only on the staggered model as a previous investigation of $[VCp_2]$ showed essentially identical results for calculations on the staggered and eclipsed forms.[5] The fully optimized, C_{2h} structure of $[CrCp_2]^+$ showed Cr−C and C−C bond lengths of 2.214 and 1.425 Å, respectively. These distances are both longer than the average Cr−C and C−C bond lengths observed in the crystal structure of $[CrCp_2][BAr^F]$ (2.195 and 1.400 Å, respectively). In our previous study of $[VCp_2]$, we observed DFT-derived V−C and C−C bond lengths to be slightly longer than those obtained from X-ray crystallography, but in excellent agreement with corresponding values from gas-phase electron diffraction studies.[5] Thus, the differences in metric parameters between the DFT- and crystallographic $[CrCp_2]^+$ structures can be attributed, to some extent, to crystal packing effects. These effects are likely more significant in the ionic $[CrCp_2]^+$ chromocenium complex as opposed to neutral [VCp2]-vanadocene. As will be seen below, the structural differences between these models have only a minor influence on calculated spectroscopic properties.

DFT Bonding Description and Spectroscopic Properties. DFT computations for both structures of $[CrCp_2]^+$ yield a $(a_{1g})^1(e_{2g})^2(e_g)^0$ configuration, with a Cr^{3+} *d*-orbital splitting pattern in qualitative agreement with that anticipated on the basis of traditional MO arguments (Figure 6 and Tables S8 and S9). In the spin unrestricted formalism, the spin-up (α) a_{1g} and e_{2g} orbitals are singly occupied, with the higher-energy, spin-up e_{1g} orbitals being unoccupied. All spin-down (β) Cr 3*d*-based MOs are unoccupied. For metallocenes, it is difficult to predict whether the a_{1g} or e_{2g} MOs are at lowest energy. The DFT computations for $[CrCp_2]^+$ predict a very small splitting for these MOs (Figure 6 and Tables S8 and S9), which agrees qualitatively with the LFT AOM analysis given above. In the α-spin manifold, the a_{1g} MO is at lowest energy, but is only ∼0.1 eV (800 cm^{-1} or 2.3 kcal/mol) lower than the e_{2g} set. The a_{1g} and e_{2g} ordering is inverted for the β-spin MOs, with the e_{2g} set lying ∼0.45 eV (3 630 cm^{-1} or 10.4 kcal/mol) below the a_{1g} MO. For the isoelectronic $[VCp_2]$ complex, we demonstrated that the magnitude of the a_{1g}−e_{2g} splitting was sensitive to the choice of density functional, with a larger splitting associated with greater Hartree−Fock character in the functional.[5] For d^3 systems such as $[VCp_2]$ and $[CrCp_2]^+$ the ordering of these MOs is inconsequential in the sense that both lead to a $^4A_{2g}$ ground state. Qualitatively, that the a_{1g} and e_{2g} MOs are close in energy means that Hund's rule is obeyed and there is no viable spin doublet ground state (or low-lying excited state). In $[CrCp_2]$, however, and later higher d-electron count $[MCp_2]^{0,+}$ species, population of the e_{1g} set is unfavorable and the ground state for $[CrCp_2]$ is a spin triplet.

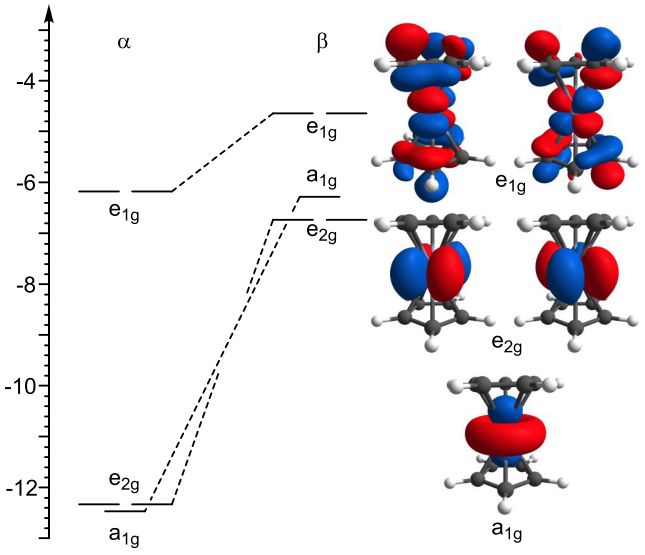

Figure 6. Energy-level diagram of the DFT-computed Cr^{3+} 3*d*-based Kohn−Sham orbitals (left) and surface contour plots of corresponding quasi-restricted orbitals for the X-ray structure of $[CrCp_2]^+$. Molecular orbital occupancies, energies, and compositions are in Tables S8 and S9.

Ground-state zero-field splitting parameters for both models of $[CrCp_2]^+$ were calculated at the coupled-perturbed (CP) DFT level of theory. Computations for the staggered (C_{2h}) and X-ray structure models of $[CrCp_2]^+$ yielded D = +3.34 cm^{-1}, in reasonable agreement with the experimental value obtained from HFEPR measurements (D = +4.82(1) cm^{-1}). The CP-

https://doi.org/10.1021/acs.organomet.5c00396
Organometallics XXXX, XXX, XXX−XXX

DFT computations predict the complex to be completely axial (E = 0), also in agreement with experiment. Overall, given the well-documented challenges of DFT methods at treating the zero-field splitting phenomenon,[79−84] the level of agreement here is as good as can be anticipated.

Given the reasonable agreement between the CP-DFT D value and its experimental counterpart, we also investigated the contributions to the calculated D value. The dominant contribution comes from spin−orbit coupling (D_{SOC}; see Table S10), as is common,[85] but not universal,[5] for transition-metal systems. In this case, the spin−spin coupling contribution (D_{SSC}) is certainly non-negligible, contributing 35% to the magnitude of D.

We used time-dependent (TD) DFT computations to predict energies for the quartet excited states of $[CrCp_2]^+$. These calculations predict the $^4A_{2g} \rightarrow {}^4E_{1g}$ (I) and $^4A_{2g} \rightarrow {}^4E_{2g}$ transitions to be very close in energy, both near 25 000 cm^{-1} (Table S10). The $^4A_{2g} \rightarrow {}^4E_{1g}$ (II) transition is predicted near 28 000 cm^{-1}. These predictions are consistent with the prominent and complicated MCD band structure from ∼23 000 to 29 000 cm^{-1}.

Multireference SORCI and CASSF/NEVPT2 Calculations. To complement our understanding of the bonding and electronic structure of $[CrCp_2]^+$ derived from DFT computations, we also performed SORCI (Spectroscopy Oriented Configuration Interaction)[86] computations on the computations on the XRD-derived model of $[CrCp_2]^+$ and CASSCF/NEVPT2 computations on both the C_{2h} and XRD-derived models of $[CrCp_2]^+$. The theory underlying these approaches, along with their strengths and limitations have been described in detail in several publications.[71,87] In short, both SORCI and CASSF/NEVPT2 methods are more successful, and substantially more reliable, than DFT approaches in calculating ground-state zero-field splitting parameters and electronic transition energies. The SORCI method, which is the more computationally demanding approach, often requires the use of truncated systems. However, the small size of $[CrCp_2]^+$ makes this system well-suited for the SORCI method. We will first discuss the results of the SORCI computations and then describe the results of the CASSCF/NEVPT2 computations by comparison.

The SORCI computations for $[CrCp_2]^+$ used as an active space three electrons in five Cr 3d orbitals and coordinates from the X-ray structure of $[CrCp_2]^+$. Although this active space is minimal, our SORCI calculations previously reported for $[VCp_2]$ showed very good agreement between experiment (D = +2.836(2) cm^{-1}) and theory (D = +2.86 cm^{-1}) using the same active space of three electrons in five 3d orbitals.[4,5] As described below, we observe little difference in CASSCF calculations using the X-ray structure of $[CrCp_2]^+$ or the DFT structure; therefore, we used the X-ray structure for the SORCI calculations. These calculations give D = +5.21 cm^{-1}, which is less than 10% higher than the experimental value, and E/D = 0. The D_{SOC} contribution is largest (4.40 cm^{-1}), with D_{SSC} contributing only 20% of the total value (0.81 cm^{-1}). The SORCI calculations provide individual contributions to the spin−orbit coupling terms (D_{SOC} and E_{SOC}) from each excited state (Table S11). These data reveal that the largest contribution to D_{SOC} comes from a $^2A_{1g}$ excited state (+3.93 cm^{-1}). The $^4E_{1g}$(1) state also contributes to D_{SOC} (+1.10 cm^{-1}). Each component of this state contributions to E_{SOC}, but these contributions are of the same magnitude but opposite sign, leading to no net contributions.

The SORCI calculations predict many doublet states from ∼13 500−17 600 cm^{-1} (Table 2). The energies for one set of $^2E_{1g}$ states coincide remarkably well with the observed MCD features at 15 800 and 15 900 cm^{-1}, lending credence to the assignment of this feature as an excitation to a doublet state rather than the $^4E_{1g}$(I) state. In addition, the SORCI calculations predict the pair of ^2A states at 15 411 cm^{-1} ($^2A_{1g}$) and 17 654 cm^{-1} ($^2A_{1g}$). Overall, the high density of doublet excited states predicted by the SORCI calculations is consistent with the complexity of the MCD spectrum from ∼15 000−19 000 cm^{-1} (Figure 5, bottom) and is also consistent with the LFT analysis (Tables S3 and S4). The SORCI calculations predict the components of the $^4E_{1g}$(I) state at 23 090 and 23 116 cm^{-1}. These energies closely match the components of the MCD pseudo-A term (23 500 and 23 710 cm^{-1}), which were determined through a Gaussian deconvolution (Table 2 and Figure S5). The deconvolution of our MCD data also revealed higher energy bands at 24 955, 26 530, and 27 460 cm^{-1}, assignments for which were uncertain. The SORCI results now allow us to assign the two lower-energy bands to the $^4E_{2g}$ state, which is predicted at 24 966 cm^{-1}. The higher-energy MCD band corresponds well with the SORCI $^4E_{1g}$(II) state that is predicted to give components at 28 388 and 28 399 cm^{-1} (Table 2).

We performed CASSCF/NEVPT2 calculations using three active spaces: CAS(3,5), CAS(3,10), and CAS(7,7). Zero-field splitting values that we discuss always include the NEVPT2 corrections. The CAS(3,5) calculations include the Cr 3d manifold (three electrons and five orbitals) in the active space. The CAS(3,10) calculations expands on this initial active space to include five Cr 4d orbitals with no additional electrons. The expansion of the metal d-shell in this manner provides added flexibility to the NEVPT2 treatment. The CAS(7,7) active space expands the initial CAS(3,5) to include the bonding counterparts to the covalent Cr-based e_{g1} MOs (Figure 2), which adds four electrons and two orbitals. As summarized in Table S10, all calculations predict D values from ∼5 to 6 cm^{-1} and E/D = 0, in excellent agreement with experiment. As differences in calculated values between the X-ray and C_{2h} model are negligible (Table S10), we will focus on the results for the X-ray model. The calculated D values decrease in magnitude from CAS(3,5) to CAS(3,10) to CAS(7,7) (6.04 to 4.64 cm^{-1}). The D value calculated for the CAS(3,5) calculations shows the poorest agreement with experiment (D = 6.04 cm^{-1}), but even this value is only ∼1.2 cm^{-1} larger than the experimental value. Thus, even with this minimally reasonable active space, the calculations perform quite well. The CAS(7,7) calculations give D = +4.74 cm^{-1} (Tables 2 and S10), essentially ideal agreement with the experimental value, D = +4.82(1) cm^{-1}. Given the excellent agreement for this latter method (within 2%), we focus on the CAS(7,7) calculations when discussing the excited state energies and contributions to D and E.

The CASSCF/NEVPT2 calculations predict a cluster of four doublet states from 14 000 to 19 000 cm^{-1} (Table 2). This prediction is in excellent agreement with the complex set of vibronic bands observed in the MCD spectrum from 15 500 to 19 000 cm^{-1} (Figure 5, bottom). The prediction of multiple bands in this region helps to rationalize the unusual behavior of the vibronic progression, which suggests at least four separate electronic transitions. For our assignments in Table 2, we have matched the experimental assignments to those excited states predicted to have the most similar energies. However, given

https://doi.org/10.1021/acs.organomet.5c00396
Organometallics XXXX, XXX, XXX−XXX

the complexity of the MCD spectrum in this region, the exact band assignments should be viewed as tentative.

The CASSCF/NEVPT2 calculations predict the components of the $^4E_{1g}(I)$ excited near 24 000 cm^{-1}, which coincides nicely with the pseudo-*A* term (derivative MCD signal) composed of bands 1 and 2 at 23 500 and 23 710 cm^{-1} (Figure 5, top and Figure S5). The calculations predict the $^4E_{2g}$ and $^2E_{1g}$ excited states to lie at slightly higher energy (26 300 and 27 000 cm^{-1}, respectively). The $^4E_{2g}$ state is thus in agreement with the intense MCD feature near 25 000 cm^{-1}. Although the pseudo-*A* term expected for the $^4E_{2g}$ excited state is not observed, this could arise from the overlap of the $^4E_{2g}$ and $^2E_{1g}$ states. The fine structure observed in this region could arise from the $^2E_{1g}$ excited state. Finally, the $^4E_{1g}(II)$ excited state is predicted at 30 300 cm^{-1}. If the CASSCF/NEVPT2 calculations overestimate the energy of the $^4E_{1g}(II)$ excited state excited state, then overlap of the transitions from the $^4E_{2g}$ and $^4E_{1g}(II)$ states would complicate the appearance of the MCD spectrum. In support, the SORCI calculations predict the $^4E_{1g}(II)$ state at the lower energy of 28 400 cm^{-1}. Thus, we propose that band 5 (at 27 460 cm^{-1}) arises from a component of the $^4E_{1g}(II)$ state.

The CASSCF/NEVPT2 calculations predict contributions to the total D_{SOC} and E_{SOC} parameters from individual excited states (Table S11). The lower-energy $^2A_{1g}$ state is the largest contributor to D_{SOC} (3.57 cm^{-1}), but has no contribution to E_{SOC}. The second-largest contributor is the $^4E_{1g}(I)$ excited state (D_{SOC} = 0.44 cm^{-1} from each component of this excited state). This state also contributes to E_{SOC}, but the two components of $^4E_{1g}(I)$ to E_{SOC} are of the same magnitude but opposite sign, leading to no net contribution. Previous calculations for $[VCp_2]$ by us[4,5] and others[88] determined that the $^2A_{1g}$ and $^4E_{1g}(I)$ provide the dominant contributions to D_{SOC} in this system as well.

CONCLUSIONS

Metallocenes of general formula $[MCp_2]^{0,+}$ are among the most iconic of organometallic species. Although chromocenium, $[CrCp_2]^+$, was first reported many years ago by E. O. Fischer in the "golden age of discovery" in metallocene chemistry,[10] relatively little attention has been paid to this Cr^{III} species over the years. It is somewhat surprising that such an iconic Cr^{III} complex should be underexplored, given the widespread use and investigation of organochromium(III) complexes in catalysis.[12−19] Work on our own V^{II} and V^{III} complexes,[89,90] led us to revisit $[VCp_2]$[4,5] and thence to prepare $[CrCp_2]^+$ using a "modern" counteranion, BAr^F,[23] to afford $[CrCp_2][BAr^F]$, **1**, and apply powerful spectroscopic techniques, HFEPR and MCD, to unravel the electronic structure of this $S = 3/2$ d^3 complex. The MCD spectra for this system are unexpectedly rich, displaying a remarkable set of vibronic progressions extending over 4000 cm^{-1}. We find that **1** is similar to $[VCp_2]$—both are rigorously axial systems, but **1** is distinctly different from its neutral isoelectronic congener in terms of its larger ZFS—the *D* value of **1** is ∼70% larger than that for $[VCp_2]$. Computational studies using both classical LFT and state of the art QCT show the basis for this difference in terms of the stronger bonding, especially π-bonding, in the Cr^{III} cationic complex versus the neutral V^{II}. LFT used crystal-field parameters as pioneered earlier,[57] but also the AOM, which is typically applied to "classical" coordination complexes with more localized bonds. Overall, it appears that the AOM is reasonably successful with respect to describing the electronic structure of both Cr^{III} and V^{II} metallocenes. The results of AOM calculations agree quite well with the CASSCF/NEVPT2 and SORCI calculations both in terms of the ZFS parameters and excited state energies (Table 2). The advantage of AOM is that the parameters are readily linked to metal−ligand bonding. In contrast, the CASSCF and SORCI results are in terms of multielectron states, the analysis of which can be challenging to relate to discrete elements of bonding. Thus, our approach highlights the complementarity of combining cutting-edge electronic structure methods with traditional approaches. We are therefore inspired and hope others will be as well to apply this methodology to other such paramagnetic metallocene complexes.

The QCT studies show a more quantitative picture of the electronic structure of **1**. First to point out is the relatively close separation between the lowest energy e_{2g} (d_{xy},$d_{x^2-y^2}$) orbitals and next highest a_{1g} (d_{z^2}) orbital (∼800 cm^{-1}; 0.1 eV for the spin-up MOs). As noted above, for d^3 metallocenes such as $[CrCp_2]^+$ and $[VCp_2]$, the relative ordering of these orbitals does not change the situation, each MO having an unpaired electron giving the ground state of $^4A_{2g}$ (in D_{5d}). Information on their relative energies, however, is helpful in understanding $[CrCp_2]$ for which its $S = 1$ ground state could be either $^3A_{2g}$ or $^3E_{2g}$, with the latter proposed many years ago.[3] The recent theoretical study on metallocenes did not explicitly address this question although they were able to calculate ^1H and ^{13}C NMR chemical shifts for $[CrCp_2]$ in good agreement with experiment.[31]

The present CASSCF and SORCI calculations not only provide unambiguous support for the $^4A_{2g}$ ground state of $[CrCp_2]^+$, they also aid in assigning its MCD spectra, which are complicated due to vibronic effects and the presence of many closely spaced electronic excited states. Specifically, the coupled analysis of the MCD data with the SORCI and CASSCF calculations allowed us to partly reassign the spectral features of this complex from the original proposal.[57] Specifically, the excited states near 16 000 cm^{-1}, which correspond to sharp, weak MCD features, are now attributed to $^2E_{1g}$ and $^2A_{1g}$ states. Both the SORCI and CASSCF calculations predict these states near 16 000 cm^{-1}. The cluster of more intense MCD features at higher energies are attributed to spin-allowed electronic transitions to the quartet excited states. These excited states show a uniform shift to higher energy compared to those of $[VCp_2]$, which could be due to the increased covalency in $[CrCp_2]^+$.

Also of interest is the ZFS in **1** which involves potentially many electronic excited states—quartet and doublet. QCT shows that only one of each is relevant. Among the quartet excited states, only $^4E_{1g}(I)$ matters, which essentially involves an electron promotion from the half-filled e_{2g} ($[d_{xy},d_{x^2-y^2}]^2$) into the empty e_{1g} orbitals. Among the many doublet excited states only a low lying $^2A_{1g}(^2G,^2D)$ matters, which involves a spin-flip within the a_{1g}^1 e_{2g}^2 ($d_{z^2}^1$,$[d_{xy},d_{x^2-y^2}]^2$) orbital occupancy and indeed has the greatest contribution to ZFS. The first process can be controlled in principle by changing the strength of π-donation by the Cp^R ligands (i.e., by electron donating or withdrawing Cp substituents) to increase or decrease the relative energy of the e_{1g} orbitals. But we suspect that control of the second process, a spin flip, is difficult to achieve by ligand design, e.g., a stronger field metallocene such as Cp* as opposed to Cp. Larger SOC (i.e., as in the shift from V to Cr) might facilitate this process. We conclude that even these long known and seemingly simple $[MCp_2]^{0,+}$ systems can

https://doi.org/10.1021/acs.organomet.5c00396
Organometallics XXXX, XXX, XXX−XXX

still hold interest in questions of electronic structure and potentially in molecular magnetism applications.

EXPERIMENTAL DETAILS

General Procedures. Unless otherwise stated, all operations were performed in a M. Braun Lab Master double-drybox under an atmosphere of purified nitrogen or using high vacuum standard Schlenk techniques under a nitrogen atmosphere. Pentane, toluene, diethyl ether (Et_2O), and dichloromethane were purchased from Fisher Scientific. Solvents were sparged with nitrogen for 20 min and dried using a two-column solvent purification system where columns designated for toluene and pentane, were packed with Q5 and alumina respectively. Columns designated for dichloromethane were packed with alumina and columns designated for benzene were packed with Q5. After drying solvents were stored over 4 Å molecular sieves. Deuterated benzene was purchased from Cambridge Isotope Laboratory (CIL). Deuterated benzene was degassed by freeze−pump−thaw cycles and stored over 4 Å molecular sieves. Celite and 4 Å molecular sieves were activated under vacuum overnight at 200 °C. Compounds $[FeCp_2][BAr^F]$ (BAr^F = tetrakis[(3,5-trifluoromethyl)-phenyl]borate) was prepared following a literature procedure,[32] but with use of $Na[BAr^F]$ prepared by a more recent method.[23] Chromocene was purchased from Strem Chemicals and recrystallized from toluene prior to use. All other reagents were purchased from either Sigma-Aldrich and Strem Chemicals and used as received. ^{19}F NMR spectra were recorded on a Bruker 300 MHz NMR spectrometer. ^{19}F NMR spectra recorded in C_6D_6 are reported with respect to external CF_3CO_2H (−78.5 ppm). Elemental analysis was performed at Robertson Microlit Laboratories, Ledgewood, NJ.

Synthesis of $[CrCp_2][BAr^F]$ (1). In a 20 mL scintillation vial containing a 5 mL orange Et_2O solution of $[CrCp_2]$ (25 mg, 0.137 mmol) was added dropwise a 5 mL blue Et_2O solution of $[FeCp_2][BAr^F]$ (144 mg, 0.137 mmol) via a glass pipet resulting in an orange solution. The solution was allowed to stir for 12 h followed by removal of all volatiles under reduced pressure, yielding an orange powder. Ferrocene was removed from the reaction mixture by the addition of pentane (5 mL) and was stirred for 30 min yielding an orange solid that was isolated on a medium porosity glass frit, washed further with 5 mL of pentane, and dried under reduced pressure yielding 131 mg of pure material. Orange single crystals of **1** were grown by layering a concentrated Et_2O solution with pentane and storing −37 °C for 16 h. Isolated yield = 91% (131 mg, 0.125 mmol). **^{19}F NMR (25 °C, 282.3 MHz, C_6D_6):** δ −58.9 ($\Delta\nu_{1/2}$ = 48.0 Hz). **Anal. Calcd. For $C_{42}H_{22}BCrF_{24}$:** C, 48.26; H, 2.12. **Found:** C, 47.99; H, 2.18; N, <0.02.

Crystallographic Details. A suitable crystal for analysis of **1** was mounted on the end of a Cryoloop coated in NVH oil and data collection was performed using a Bruker APEXII CCD area detector employing Mo Kα radiation (graphite monochromator) at a temperature of 100 K. Rotation frames were integrated using SAINT,[91] producing a listing of unaveraged F^2 and $\sigma(F^2)$ values which were then passed to the SHELXTL[92] program package for further processing and structure solution. The intensity data were corrected for Lorentz and polarization effects and for absorption using SADABS.[93] The structure was solved by direct methods using SHELXS-97.[94,95] Refinement was by full-matrix least-squares based on F^2 using SHELXL-97.[94,95] All reflections were used during refinements. Non-hydrogen atoms were refined anisotropically and hydrogen atoms were refined using a riding model.

EPR Spectroscopy. X-band EPR spectra of **1** were recorded on a modified Varian E-109 spectrometer at 77 K. EPR simulations for $S' = 1/2$ used the program QPOW by Belford[96] (modified by J. Telser) and for $S = 3/2$ used the program SPIN by A. Ozarowski, with a standard spin Hamiltonian for $S = 3/2$.[97]

HFEPR Spectroscopy. HFEPR data were acquired at the EMR Facility of the NHMFL using a spectrometer previously described,[98] but modified by the use of low-frequency sources followed by a chain of amplifiers and frequency multipliers (VDI Inc., Charlottesville, VA), which operate in the frequency range of 50−420 GHz.

MCD Spectroscopy. Magnetic circular dichroism (MCD) spectra were collected using a spectropolarimeter (Jasco J-815) interfaced with a magneto-optical cryostat (Oxford Instruments SM 4000−8). Data were collected for solid samples of $[CrCp_2][BAr^F]$ prepared as a mull in Fluorolube.

Computational Methods. Ligand Field Theory (LFT) calculations employed the locally written (J. Telser)[99] programs DDN and DDNFIT and the program Ligfield by J. Bendix.[100] All Quantum Chemical Theory (QCT) calculations were performed using ORCA 5.04.[101−103] Calculations were performed using the X-ray structure coordinates, with the positions of the hydrogen atoms optimized using density functional theory (DFT) methods. These calculations employed the BP functional[104,105] and def2-TZVP (Cr, C, and H) basis sets.[106,107] The resolution of the identity (RI) approximation was used to speed the calculations.[108] Orbitals were visualized using ChemCraft.[109] Electronic transition energies were calculated by the time-dependent (TD) DFT method,[110,111] the SORCI method,[86,87,112] and the CASSCF/NEVPT2 method.[113−116] The SORCI and CASSCF methods was also used to calculate ground-state spin Hamiltonian parameters. The CASSCF calculations used several active spaces, as described in the text. These calculations included 10 quartet roots and 40 doublet roots and def2-TZVP basis sets for all atoms, with the def2-TZVP/C and def2/J auxiliary basis sets used with the RIJCOSX approximation. The SORCI calculations used parameters previously described for $[VCp_2]$.[4]

ASSOCIATED CONTENT

Supporting Information

The Supporting Information is available free of charge at https://pubs.acs.org/doi/10.1021/acs.organomet.5c00396.

Additional crystallographic, EPR, and MCD figures, tables of LFT and QCT results (PDF)

Accession Codes

Deposition Number 2492498 contains the supplementary crystallographic data for this paper. These data can be obtained free of charge via the joint Cambridge Crystallographic Data Centre (CCDC) and Fachinformationszentrum Karlsruhe Access Structures service.

AUTHOR INFORMATION

Corresponding Authors

Daniel J. Mindiola − *Department of Chemistry, University of Pennsylvania, Philadelphia, Pennsylvania 19104, United States;* orcid.org/0000-0001-8205-7868; Email: mindiola@sas.upenn.edu

Timothy A. Jackson − *Department of Chemistry, University of Kansas, Lawrence, Kansas 66045, United States;* orcid.org/0000-0002-3529-2715; Email: taj@ku.edu

Joshua Telser − *Department of Biological, Physical and Health Sciences, Roosevelt University, Chicago, Illinois 60605, United States;* orcid.org/0000-0003-3307-2556; Email: jtelser@roosevelt.edu

Authors

Keith A. Searles − *Department of Chemistry, University of Pennsylvania, Philadelphia, Pennsylvania 19104, United States;* Present Address: Department of Chemistry, University of Florida, Gainesville, Florida 32611−7200, United States; orcid.org/0000-0003-2976-3960

J. Krzystek − *National High Magnetic Field Laboratory, Florida State University, Tallahassee, Florida 32310, United States;* orcid.org/0000-0001-6088-1936

Gayan B. Wijeratne − *Department of Chemistry, University of Kansas, Lawrence, Kansas 66045, United States;* Present Address: Department of Chemistry, University of

https://doi.org/10.1021/acs.organomet.5c00396
Organometallics XXXX, XXX, XXX−XXX

Alabama, Tuscaloosa, Alabama 35487−0336, United States; orcid.org/0000-0001-7609-6406

Patrick J. Carroll − *Department of Chemistry, University of Pennsylvania, Philadelphia, Pennsylvania 19104, United States*

Complete contact information is available at: https://pubs.acs.org/10.1021/acs.organomet.5c00396

Notes

The authors declare no competing financial interest.

■ ACKNOWLEDGMENTS

D.J.M. thanks the U.S. National Science Foundation (NSF; grants CHE-2453436, CHE-2154620, CHE-1152123, and MCB-1908587) and the University of Pennsylvania for funding. T.A.J. thanks the NSF for support (grant CHE-2453075). A portion of this work was performed at the National High Magnetic Field Laboratory, which is supported by the NSF (Cooperative Agreement No. DMR-2128556) and the State of Florida. J.T. thanks Prof. Brian M. Hoffman, Northwestern University, for use of an X-band EPR spectrometer which is supported by the NSF through grant CHE-2333907 to B.M.H. We thank Dr. Michael Gau, U. of Pennsylvania, for assistance with analysis of x-ray crystallographic data. We thank Prof. Jesper Bendix, U. of Copenhagen, Denmark, for Ligfield software and Dr. Andrew Ozarowski, NHMFL, for SPIN (EPR simulation) software.

■ REFERENCES

(1) Ernst, R. D. Structural and reactivity patterns in transition-metal-pentadienyl chemistry. *Chem. Rev.* **1988**, *88*, 1255−1291.

(2) Laszlo, P.; Hoffmann, R. Ferrocene: Ironclad History or Rashomon Tale? *Angew. Chem., Int. Ed.* **2000**, *39*, 123−124.

(3) König, E.; Schnakig, R.; Kanellakopulos, B.; Klenze, R. Magnetism down to 0.90 K, zero-field splitting, and the ligand field in chromocene. *Chem. Phys. Lett.* **1977**, *50*, 439−441.

(4) Jackson, T. A.; Krzystek, J.; Ozarowski, A.; Wijeratne, G. B.; Wicker, B. F.; Mindiola, D. J.; Telser, J. Addition to Vanadocene de Novo: Spectroscopic and Computational Analysis of Bis(η5-cyclopentadienyl)vanadium(II). *Organometallics* **2014**, *33*, 1325.

(5) Jackson, T. A.; Krzystek, J.; Ozarowski, A.; Wijeratne, G. B.; Wicker, B. F.; Mindiola, D. J.; Telser, J. Vanadocene *de Novo*: Spectroscopic and Computational Analysis of Bis(η^5-cyclopentadienyl)vanadium(II). *Organometallics* **2012**, *31*, 8265−8274.

(6) Prins, R. Electronic structure of the ferricenium cation. *Mol. Phys.* **1970**, *19*, 603−620.

(7) Rajasekharan, M. V.; Bucher, R.; Deiss, E.; Zoller, L.; Salzer, A. K.; Moser, E.; Weber, J.; Ammeter, J. H. ESR study of the electronic structure and dynamic Jahn-Teller effect in nickelocenium cation. *J. Am. Chem. Soc.* **1983**, *105*, 7516−7522.

(8) Malischewski, M.; Adelhardt, M.; Sutter, J.; Meyer, K.; Seppelt, K. Isolation and structural and electronic characterization of salts of the decamethylferrocene dication. *Science* **2016**, *353*, No. 678.

(9) Kub, N. G.; Sievers, R.; Reimann, M.; Streit, T.-N.; Steinhauer, S.; Schlögl, J.; Kaupp, M.; Malischewski, M. Coexistence of Metallocene Cations and Anions. *J. Am. Chem. Soc.* **2025**, *147*, 34641−34646.

(10) Fischer, E. O.; Ulm, K. Über Aromatenkomplexe von Metallen, LV. Zur Kenntnis des Di-cyclopentadienyl-chrom(III)-Kations. *Chem. Ber.* **1962**, *95*, 692−694.

(11) Staples, O.; Reinholdt, A.; Mindiola, D. J. 4.13-Chromium(III) Complexes. In *Comprehensive Coordination Chemistry III*; Constable, E. C.; Parkin, G.; Que, L., Jr., Eds.; Elsevier: Oxford, 2021; pp 508−551.

(12) Thomas, B. J.; Theopold, K. H. Cationic chromium(III) alkyls as olefin polymerization catalysts. *J. Am. Chem. Soc.* **1988**, *110*, 5902−5903.

(13) Severn, J. R.; Chadwick, J. C.; Duchateau, R.; Friederichs, N. "Bound but Not Gagged" - Immobilizing Single-Site α-Olefin Polymerization Catalysts. *Chem. Rev.* **2005**, *105*, 4073−4147.

(14) Jones, D. J.; Gibson, V. C.; Green, S. M.; Maddox, P. J.; White, A. J. P.; Williams, D. J. Discovery and Optimization of New Chromium Catalysts for Ethylene Oligomerization and Polymerization Aided by High-Throughput Screening. *J. Am. Chem. Soc.* **2005**, *127*, 11037−11046.

(15) Xu, T.; Mu, Y.; Gao, W.; Ni, J.; Ye, L.; Tao, Y. Highly Active Half-Metallocene Chromium(III) Catalysts for Ethylene Polymerization Activated by Trialkylaluminum. *J. Am. Chem. Soc.* **2007**, *129*, 2236−2237.

(16) Albahily, K.; Fomitcheva, V.; Shaikh, Y.; Sebastiao, E.; Gorelsky, S. I.; Gambarotta, S.; Korobkov, I.; Duchateau, R. New Self-Activating Organochromium Catalyst Precursor for Selective Ethylene Trimerization. *Organometallics* **2011**, *30*, 4201−4210.

(17) Trummer, D.; Nobile, A. G.; Payard, P.-A.; Ashuiev, A.; Kakiuchi, Y.; Klose, D.; Jeschke, G.; Copéret, C. Union carbide polymerization catalysts: from uncovering active site structures to designing molecularly-defined analogs. *Chem. Sci.* **2022**, *13*, 11091−11098.

(18) Hansen, H.-B.; Krzystek, J.; Telser, J.; Swain, A.; Rajaraman, G.; Wadepohl, H.; Enders, M. Solid-State Conformational Isomerism Lacking a Gas-Phase Energy Barrier: Its Structural, Spectroscopic, and Theoretical Identification in an Organochromium(III) Complex. *Organometallics* **2022**, *41*, 1558−1564.

(19) Hirscher, N. A.; Arnett, C. H.; Oyala, P. H.; Agapie, T. Characterization of Cr-Hydrocarbyl Species via Pulse EPR in the Study of Ethylene Tetramerization Catalysis. *Organometallics* **2020**, *39*, 4420−4429.

(20) Pasynskii, A. A.; Eremenko, I. L.; Abdullaev, A. S.; Orazsakhatov, B.; Nefedov, S. E.; Stomakhina, E. E.; Ellert, O. G.; Katser, S. B.; Yanovskii, A. I.; Struchkov, Y. T. Thiolate Derivatives of Vanadocene: Synthesis, Magnetic Properties and Molecular Structures of Cp_2VSPh, $Cp_2VSC_6H_2(CMe_3)_2(OH)$, $(MeC_5H_4)_2V(\mu^3\text{-}S)Fe_2(CO)_6(\mu^3\text{-}S)V(MeC_5H_4)_2$, and also $Cp_2Cr^+CpCr(CO)_3^-$. *Russ. J. Inorg. Chem.* **1990**, *35*, 2257−2264.

(21) Doerrer, L. H.; Green, M. L. H. Oxidation of $[M(\eta\text{-}C_5H_5)_2]$, M = Cr, Fe or Co, by the new Brønsted acid $H_2O{\cdot}B(C_6F_5)_3$ yielding the salts $[M(\eta\text{-}C_5H_5)_2]^+A'$, where A^- = $[(C_6F_5)_3B(\mu\text{-}OH)B(C_6F_5)_3]^-$ or $[(C_6F_5)_3BOH\cdots H_2OB(C_6F_5)_3]^-$. *J. Chem. Soc., Dalton Trans.* **1999**, 4325−4329.

(22) Burin, M. E.; Smirnova, M. V.; Fukin, G. K.; Baranov, E. V.; Bochkarev, M. N. Neodymium(II) and Dysprosium(II) Iodides in the Reactions with Metallocenes of d-Transition Metals. *Eur. J. Inorg. Chem.* **2006**, *2006*, 351−356.

(23) Yakelis, N. A.; Bergman, R. G. Safe Preparation and Purification of Sodium Tetrakis[(3,5-trifluoromethyl)phenyl]borate ($NaBArF_{24}$): Reliable and Sensitive Analysis of Water in Solutions of Fluorinated Tetraarylborates. *Organometallics* **2005**, *24*, 3579−3581.

(24) Krzystek, J.; Kohl, G.; Hansen, H.-B.; Enders, M.; Telser, J. Combining HFEPR and NMR Spectroscopies to Characterize Organochromium(III) Complexes with Large Zero-Field Splitting. *Organometallics* **2019**, *38*, 2179−2188.

(25) Neese, F.; Solomon, E. I. MCD *C*-term Signs, Saturation Behavior, and Determination of Band Polarizations in Randomly Oriented Systems with Spin $S \geq 1/2$. Application to $S = 1/2$ and $S = 5/2$. *Inorg. Chem.* **1999**, *38*, 1847−1865.

(26) Kirk, M. L.; Peariso, K. Recent applications of MCD spectroscopy to metalloenzymes. *Curr. Opin. Chem. Biol.* **2003**, *7*, 220−227.

(27) Decker, A.; Rohde, J.-U.; Que, L., Jr.; Solomon, E. I. Spectroscopic and Quantum Chemical Characterization of the Electronic Structure and Bonding in a Non-Heme $Fe^{IV}O$ Complex. *J. Am. Chem. Soc.* **2004**, *126*, 5378−5379.

(28) Decker, A.; Rohde, J.-U.; Klinker, E. J.; Wong, S. D.; Que, L., Jr.; Solomon, E. I. Spectroscopic and Quantum Chemical Studies on Low-Spin $Fe^{IV}O$ Complexes: Fe−O Bonding and Its Contributions to Reactivity. *J. Am. Chem. Soc.* **2007**, *129*, 15983−15996.
(29) Srnec, M.; Wong, S. D.; England, J.; Que, L., Jr.; Solomon, E. I. π-Frontier molecular orbitals in S = 2 ferryl species and elucidation of their contributions to reactivity. *Proc. Natl. Acad. Sci. U.S.A.* **2012**, *109*, 14326−14331.
(30) Srnec, M.; Wong, S. D.; Matthews, M. L.; Krebs, C.; Bollinger, J. M., Jr.; Solomon, E. I. Electronic Structure of the Ferryl Intermediate in the α-Ketoglutarate Dependent Non-Heme Iron Halogenase SyrB2: Contributions to H Atom Abstraction Reactivity. *J. Am. Chem. Soc.* **2016**, *138*, 5110−5122.
(31) Rouf, S. A.; Mareš, J.; Vaara, J. Relativistic Approximations to Paramagnetic NMR Chemical Shift and Shielding Anisotropy in Transition Metal Systems. *J. Chem. Theory Comput.* **2017**, *13*, 3731−3745.
(32) Chávez, I.; Alvarez-Carena, A.; Molins, E.; Roig, A.; Maniukiewicz, W.; Arancibia, A.; Arancibia, V.; Brand, H.; Manuel Manríquez, J. Selective oxidants for organometallic compounds containing a stabilising anion of highly reactive cations: $(3,5\text{-}(CF_3)_2C_6H_3)_4B^-)Cp_2Fe^+$ and $(3,5(CF_3)_2C_6H_3)_4B^-)Cp^*_2Fe^+$. *J. Organomet. Chem.* **2000**, *601*, 126−132.
(33) Gard, E.; Haaland, A.; Novak, D. P.; Seip, R. The molecular structures of dicyclopentadienylvanadium, $(C_5H_5)_2V$, and dicyclopentadienylchromium, $(C_5H_5)_2Cr$, determined by gas phase electron diffraction. *J. Organomet. Chem.* **1975**, *88*, 181−189.
(34) Antipin, M. Y.; Boese, R. Structure of Vanadocene in the Temperature Interval 108 - 357 K and the Nature of the Ring Disorder. *Acta Crystallogr., Sect. B:Struct. Sci.* **1996**, *52*, 314−322.
(35) There is a very early crystal structure by Weiss and Fischer, but it does not provide atomic coordinates (CSD: CYCPCR).
(36) Weiss, E.; Fischer, E. O. Zur Kristallstruktur von Dicyclopentadienyl-chrom(II). *Z. Anorg. Allg. Chem.* **1956**, *284*, 69−72.
(37) Flower, K. R.; Hitchcock, P. B. Crystal and molecular structure of chromocene $(\eta^5\text{-}C_5H_5)_2Cr$. *J. Organomet. Chem.* **1996**, *507*, 275−277.
(38) Miller, J. S.; McLean, R. S.; Vazquez, C.; Calabrese, J. C.; Zuo, F.; Epstein, A. J. Decamethylchromocenium tetracyanoethenide, $[Cr(C_5Me_5)_2]^{\cdot+}[TCNE]^+$: a molecular ferromagnet with T_c= 3.65 K. *J. Mater. Chem.* **1993**, *3*, 215−218.
(39) Kaul, B. B.; Durfee, W. S.; Yee, G. T. Dialkyldicyanofumarate Diesters: Tunable Building Blocks for Molecule-Based Ferromagnets. *J. Am. Chem. Soc.* **1999**, *121*, 6862−6866.
(40) Kaul, B. B.; Sommer, R. D.; Noll, B. C.; Yee, G. T. Synthesis, Structure, and Magnetic Properties of the Charge-Transfer Salt Ferromagnet Decamethylchromocenium Dimethyl Dicyanofumarate, T_{Curie} = 5.7 K. *Inorg. Chem.* **2000**, *39*, 865−868.
(41) Konarev, D. V.; Khasanov, S. S.; Otsuka, A.; Saito, G. The Reversible Formation of a Single-Bonded $(C_{60}^-)_2$ Dimer in Ionic Charge Transfer Complex: $Cp^*_2Cr{\cdot}C_{60}(C_6H_4Cl_2)_2$. The Molecular Structure of $(C_{60}^-)_2$. *J. Am. Chem. Soc.* **2002**, *124*, 8520−8521.
(42) Konarev, D. V.; Khasanov, S. S.; Saito, G.; Otsuka, A.; Yoshida, Y.; Lyubovskaya, R. N. Formation of Single-Bonded $(C_{60}^-)_2$ and $(C_{70}^-)_2$ Dimers in Crystalline Ionic Complexes of Fullerenes. *J. Am. Chem. Soc.* **2003**, *125*, 10074−10083.
(43) Wang, G.; Slebodnick, C.; Butcher, R. J.; Tam, M. C.; Crawford, T. D.; Yee, G. T. A Family of Decamethylmetallocene Charge-Transfer Salt Magnets Using Methyl Tricyanoethylenecarboxylate (MTCE) as the Electron Acceptor. *J. Am. Chem. Soc.* **2004**, *126*, 16890−16895.
(44) Semenov, N. A.; Pushkarevsky, N. A.; Lonchakov, A. V.; Bogomyakov, A. S.; Pritchina, E. A.; Suturina, E. A.; Gritsan, N. P.; Konchenko, S. N.; Mews, R.; Ovcharenko, V. I.; Zibarev, A. V. Heterospin π-Heterocyclic Radical-Anion Salt: Synthesis, Structure, and Magnetic Properties of Decamethylchromocenium [1,2,5]-Thiadiazolo[3,4-*c*][1,2,5]thiadiazolidyl. *Inorg. Chem.* **2010**, *49*, 7558−7564.
(45) Konarev, D. V.; Zorina, L. V.; Khasanov, S. S.; Hakimova, E. z. U.; Lyubovskaya, R. N. Structure and magnetic properties of ionic compound $(Cp^*_2Cr^+){\cdot}(Fe^IPc^-){\cdot}(C_6H_4Cl_2)_4$ containing negatively charged iron phthalocyanine. *New J. Chem.* **2012**, *36*, 48−51.
(46) Robbins, J. L.; Edelstein, N.; Spencer, B.; Smart, J. C. Syntheses and electronic structures of decamethylmetallocenes. *J. Am. Chem. Soc.* **1982**, *104*, 1882−1893.
(47) Aldridge, S.; Shang, M.; Fehlner, T. P. Structure of the Chromium(III) Salt $[Cp^*_2Cr]^+[Cp^*CrCl_3]$. *Acta Crystallogr., Sect. C: Cryst. Struct. Commun.* **1998**, *54*, 47−49.
(48) C1−5 to C35−40 centroid distance is 3.7819(13) Å and C6−10 to C27−32 centroid distance is 3.746(5)Å
(49) Fortman, G. C.; Kégl, T.; Li, Q.-S.; Zhang, X.; Schaefer, H. F.; Xie, Y.; King, R. B.; Telser, J.; Hoff, C. D. Spectroscopic Detection and Theoretical Confirmation of the Role of $Cr_2(CO)_5(C_5R_5)_2$ and ·$Cr(CO)_2$(ketene)(C_5R_5) as Intermediates in Carbonylation of $NNCHSiMe_3$ to $OCCHSiMe_3$ by ·$Cr(CO)_3(C_5R_5)$ (R = H, CH_3). *J. Am. Chem. Soc.* **2007**, *129*, 14388−14400.
(50) Prins, R.; Reinders, F. J. Electron spin resonance measurements of dibenzenechromium cation. *Chem. Phys. Lett.* **1969**, *3*, 45−48.
(51) Ammeter, J. H. EPR of orbitally degenerate sandwich compounds. *J. Magn. Reson.* **1978**, *30*, 299−325.
(52) For a given species, more than one $g'_\perp$ value was reported, e.g., $Cp^*_2Cr{\cdot}C_{60}{\cdot}(C_6H_4Cl_2)_2$ gave $g'_\perp$ = 3.974, 3.728, 3.467.
(53) Krzystek, J.; Zvyagin, S. A.; Ozarowski, A.; Trofimenko, S.; Telser, J. Tunable-frequency high-field electron paramagnetic resonance. *J. Magn. Reson.* **2006**, *178*, 174−183.
(54) Telser, J.; Ozarowski, A.; Krzystek, J. High-Frequency and -Field Electron Paramagnetic Resonance of Transition Metal ion (d block) Coordination Complexes. In *Electron Paramagnetic Resonance*; The Royal Society of Chemistry, 2013; Vol. *23*, pp 209−263.
(55) Telser, J.; Krzystek, J.; Ozarowski, A. High-frequency and high-field electron paramagnetic resonance (HFEPR): a new spectroscopic tool for bioinorganic chemistry. *JBIC, J. Biol. Inorg. Chem.* **2014**, *19*, 297−318.
(56) Above 28 500 cm^{-1} the MCD signal no longer showed field- or temperature-dependent behavior consistent with MCD *C*-terms. This lack of *C*-term signal at high energy is likely due to low light transmission through the mull sample at these high frequencies.
(57) Pavlík, I.; Černý, V.; Maxová, E. On the chemistry of sandwich complexes. XVI. The ligand field theory for dicyclopentadienyl d^3 and d^7 complexes. The d-d transitions and ligand field parameters of vanadocene and some complexes of Cr(III). *Collect. Czech. Chem. Commun.* **1972**, *37*, 171−195.
(58) Aleksanyan, V. T.; Lokshin, B. V.; Borisov, G. K.; Devyatykh, G. G.; Smirnov, A. S.; Nazarova, R. V.; Koningstein, J. A.; Gächter, B. F. Raman spectra of cyclopentadienyl complexes $(\eta^5\text{-}C_5H_5)_2M$ (M = Mn, Cr, V, Ru, Os). *J. Organomet. Chem.* **1977**, *124*, 293−298.
(59) Aleksanyan, V. T.; Greenwald, I. I. Investigation of charge separation in dicyclopentadienyl complexes of metals by theoretical analysis of infrared intensities. *J. Mol. Struct.* **1982**, *90*, 35−47.
(60) Kemner, E.; de Schepper, I. M.; Kearley, G. J.; Jayasooriya, U. A. The vibrational spectrum of solid ferrocene by inelastic neutron scattering. *J. Chem. Phys.* **2000**, *112*, 10926−10929.
(61) Adams, D. M.; Fernando, W. S. The vibrational spectrum of ruthenocene. *J. Chem. Soc., Dalton Trans.* **1972**, 2507−2511.
(62) The two equivalent Cp(unit)-M bonds transform as A_{1g} + A_{2u} in D_{5d} and are respectively ν_4 and ν_{11}
(63) Brunold, T. C.; Tamura, N.; Kitajima, N.; Moro-oka, Y.; Solomon, E. I. Spectroscopic Study of $[Fe_2(O_2)(OBz)_2\{HB(pz')_3\}_2]$: Nature of the μ-1,2 Peroxide−Fe(III) Bond and Its Possible Relevance to O_2 Activation by Non-Heme Iron Enzymes. *J. Am. Chem. Soc.* **1998**, *120*, 5674−5690.
(64) Jackson, T. A.; Xie, J.; Yikilmaz, E.; Miller, A.-F.; Brunold, T. C. Spectroscopic and Computational Studies on Iron and Manganese Superoxide Dismutases: Nature of the Chemical Events Associated with Active-Site pKs. *J. Am. Chem. Soc.* **2002**, *124*, 10833−10845.

https://doi.org/10.1021/acs.organomet.5c00396
Organometallics XXXX, XXX, XXX−XXX

(65) We shall refer to the isolated cation investigated by computational studies as $[CrCp_2]^+$ and employ **1** to refer to the experimentally studied BAr^F salt.
(66) Ballhausen, C. J. *Introduction to Ligand Field Theory*; McGraw-Hill: New York, 1962; pp 99−103.
(67) Warren, K. D. Ligand Field Theory of Metal Sandwich Complexes. In *Bonding Forces*; Springer: Berlin, Heidelberg, 1976; pp 45−159.
(68) Bendix, J.; Brorson, M.; Schäffer, C. E. Accurate empirical spin orbit coupling parameters z_{nd} for gaseous nd^q transition metal ions. The parametrical multiplet term model. *Inorg. Chem.* **1993**, *32*, 2838−2849.
(69) Brorson, M.; Schäffer, C. E. Orthonormal interelectronic repulsion operators in the parametrical d^q model. Application of the model to gaseous ions. *Inorg. Chem.* **1988**, *27*, 2522−2530.
(70) Schmidtke, H.-H. The Variation of Slater-Condon Parameters F^k and Racah Parameters *B* and *C* with Chemical Bonding in Transition Group Complexes. In *Optical Spectra and Chemical Bonding in Inorganic Compounds: Special Vol. dedicated to Professor Jørgensen I*; Mingos, D. M. P.; Schönherr, T., Eds.; Springer: Berlin, Heidelberg, 2004; pp 19−35.
(71) Atanasov, M.; Ganyushin, D.; Sivalingam, K.; Neese, F. A Modern First-Principles View on Ligand Field Theory Through the Eyes of Correlated Multireference Wavefunctions. In *Molecular Electronic Structures of Transition Metal Complexes II*; Mingos, D. M. P.; Day, P.; Dahl, J. P., Eds.; Springer: Berlin, Heidelberg, 2012; pp 149−220.
(72) Neese, F. Importance of Direct Spin-Spin Coupling and Spin-Flip Excitations for the Zero-Field Splittings of Transition Metal Complexes: A Case Study. *J. Am. Chem. Soc.* **2006**, *128*, 10213−10222.
(73) Schäffer, C. E. A Perturbation Representation of Weak Covalent Bonding. In *Structure and Bonding*; Springer, 1968; Vol. *5*, pp 68−95 .
(74) Schönherr, T.; Atanasov, M.; Adamsky, H. Angular Overlap Model. In *In Comprehensive Coordination Chemistry II*; McCleverty, J. A.; Meyer, T. J., Eds.; Pergamon: Oxford, 2003; pp 443−455.
(75) Miessler, G. L.; Fischer, P. J.; Tarr, D. A. *Inorganic Chemistry*. 5th ed.; Pearson: Upper Saddle River, NJ, 2014.
(76) Nagelski, A. L.; Ozerov, M.; Fataftah, M. S.; Krzystek, J.; Greer, S. M.; Holland, P. L.; Telser, J. Electronic Structure of Three-Coordinate Fe^{II} and Co^{II} β-Diketiminate Complexes. *Inorg. Chem.* **2024**, *63*, 4511−4526.
(77) Reinholdt, A.; Pividori, D.; Laughlin, A. L.; DiMucci, I. M.; MacMillan, S. N.; Jafari, M. G.; Gau, M. R.; Carroll, P. J.; Krzystek, J.; Ozarowski, A.; Telser, J.; Lancaster, K. M.; Meyer, K.; Mindiola, D. J. A Mononuclear and High-Spin Tetrahedral Ti^{II} Complex. *Inorg. Chem.* **2020**, *59*, 17834−17850.
(78) Schweinfurth, D.; Krzystek, J.; Atanasov, M.; Klein, J.; Hohloch, S.; Telser, J.; Demeshko, S.; Meyer, F.; Neese, F.; Sarkar, B. Tuning Magnetic Anisotropy Through Ligand Substitution in Five-Coordinate Co(II) Complexes. *Inorg. Chem.* **2017**, *56*, 5253−5265.
(79) Zolnhofer, E. M.; Wijeratne, G. B.; Jackson, T. A.; Fortier, S.; Heinemann, F. W.; Meyer, K.; Krzystek, J.; Ozarowski, A.; Mindiola, D. J.; Telser, J. Electronic Structure and Magnetic Properties of a Titanium(II) Coordination Complex. *Inorg. Chem.* **2020**, *59*, 6187−6201.
(80) Liakos, D. G.; Ganyushin, D.; Neese, F. A Multiconfigurational ab Initio Study of the Zero-Field Splitting in the Di- and Trivalent Hexaquo−Chromium Complexes. *Inorg. Chem.* **2009**, *48*, 10572−10580.
(81) Ye, S.; Neese, F.; Ozarowski, A.; Smirnov, D.; Krzystek, J.; Telser, J.; Liao, J.-H.; Hung, C.-H.; Chu, W.-C.; Tsai, Y.-F.; Wang, R.-C.; Chen, K.-Y.; Hsu, H.-F. Family of V(III)-Tristhiolato Complexes Relevant to Functional Models of Vanadium Nitrogenase: Synthesis and Electronic Structure Investigations by Means of High-Frequency and -Field Electron Paramagnetic Resonance Coupled to Quantum Chemical Computations. *Inorg. Chem.* **2010**, *49*, 977−988.
(82) Zein, S.; Duboc, C.; Lubitz, W.; Neese, F. A Systematic Density Functional Study of the Zero-Field Splitting in Mn(II) Coordination Compounds. *Inorg. Chem.* **2008**, *47*, 134−142.
(83) Maganas, D.; Sottini, S.; Kyritsis, P.; Groenen, E. J. J.; Neese, F. Theoretical Analysis of the Spin Hamiltonian Parameters in $Co^{(II)}S_4$ Complexes, Using Density Functional Theory and Correlated ab initio Methods. *Inorg. Chem.* **2011**, *50*, 8741−8754.
(84) Leto, D. F.; Massie, A. A.; Colmer, H. E.; Jackson, T. A. X-Band Electron Paramagnetic Resonance Comparison of Mononuclear Mn^{IV}-oxo and Mn^{IV}-hydroxo Complexes and Quantum Chemical Investigation of Mn^{IV} Zero-Field Splitting. *Inorg. Chem.* **2016**, *55*, 3272−3282.
(85) Ganyushin, D.; Gilka, N.; Taylor, P. R.; Marian, C. M.; Neese, F. The resolution of the identity approximation for calculations of spin-spin contribution to zero-field splitting parameters. *J. Chem. Phys.* **2010**, *132*, 144111.
(86) Schapiro, I.; Neese, F. SORCI for photochemical and thermal reaction paths: A benchmark study. *Comput. Theor. Chem.* **2014**, *1040−1041*, 84−98.
(87) Neese, F. A spectroscopy oriented configuration interaction procedure. *J. Chem. Phys.* **2003**, *119*, 9428−9443.
(88) Prins, R.; Van Voorst, J. D. W. Bonding in Sandwich Compounds. *J. Chem. Phys.* **1968**, *49*, 4665−4673.
(89) Andino, J. G.; Kilgore, U. J.; Pink, M.; Ozarowski, A.; Krzystek, J.; Telser, J.; Baik, M.-H.; Mindiola, D. J. Intermolecular C−H bond activation of benzene and pyridines by a vanadium(III) alkylidene including a stepwise conversion of benzene to a vanadium-benzyne complex. *Chem. Sci.* **2010**, *1*, 351−356.
(90) Tran, B. L.; Krzystek, J.; Ozarowski, A.; Chen, C.-H.; Pink, M.; Karty, J. A.; Telser, J.; Meyer, K.; Mindiola, D. J. Formation and Reactivity of the Terminal Vanadium Nitride Functionality. *Eur. J. Inorg. Chem.* **2013**, *2013*, 3916−3929.
(91) Bruker-AXS. *SAINT Software User's Guide, Version 7.34a*; Bruker AXS, Inc: Madison, Wisconsin, USA, 2005.
(92) Sheldrick, G. M. *SHELXTL, Version 6.12*; Bruker AXS, Inc: Madison, WI, 2001.
(93) Bruker-AXS. *SADABS, Verson 2012/1*; Bruker AXS, Inc: Madison, Wisconsin, USA, 2012.
(94) Sheldrick, G. M. A short history of SHELX. *Acta Crystallogr., Sect. A:Found. Crystallogr.* **2008**, *64*, 112−122.
(95) Sheldrick, G. M. Crystal structure refinement with SHELXL. *Acta Crystallogr., Sect. C:Struct. Chem.* **2015**, *C71*, 3−8.
(96) Belford, R. L.; Belford, G. G. Eigenfield expansion technique for efficient computation of field-swept fixed-frequency spectra from relaxation master equations. *J. Chem. Phys.* **1973**, *59*, 853−854.
(97) Abragam, A.; Bleaney, B. *Electron Paramagnetic Resonance of Transition Ions (Oxford Classic Texts in the Physical Sciences)*; Oxford University Press: Oxford, UK, 2012.
(98) Hassan, A. K.; Pardi, L. A.; Krzystek, J.; Sienkiewicz, A.; Goy, P.; Rohrer, M.; Brunel, L.-C. Ultrawide band multifrequency high-field EMR technique: a methodology for increasing spectroscopic information. *J. Magn. Reson.* **2000**, *142*, 300−312.
(99) Telser, J. *DDN and other Software*; Max Planck Digital Library: Mülheim a.d. Ruhr, Germany, 2025 DOI: 10.17617/3.XNQCUE.
(100) Bendix, J. Ligfield. In *Comprehensive Coordination Chemistry II, Vol. 2: Fundamentals: Physical Methods, Theoretical Analysis, and Case Studies*; Lever, A. B. P., Ed.; Elsevier: Amsterdam, 2003; Vol. *2*, pp 673−676.
(101) Neese, F. Software update: the ORCA program system, version 4.0. *WIREs Comput. Mol. Sci.* **2018**, *8*, No. e1327.
(102) Neese, F. *ORCA—an Ab Initio, Density Functional and Semiempirical Program Package*; Max Planck Institut für Chemische Energiekonversion: Mülheim an der Ruhr, Germany, 2014.
(103) Neese, F. The ORCA program system. *WIREs Comput. Mol. Sci.* **2012**, *2*, 73−78.
(104) Becke, A. D. Density Functional Calculations of Molecular Bond Energies. *J. Chem. Phys.* **1986**, *84*, 4524−4529.

https://doi.org/10.1021/acs.organomet.5c00396
Organometallics XXXX, XXX, XXX−XXX

(105) Perdew, J. P. Density Functional Approximation for the Correlation Energy of the Inhomogeneous Electron Gas. *Phys. Rev. B* **1986**, *33*, 8822−8824.
(106) Schäfer, A.; Huber, C.; Ahlrichs, R. Fully Optimized Contracted Gaussian Basis Sets of Triple Zeta Valence Quality for Atoms Li to Kr. *J. Chem. Phys.* **1994**, *100*, 5829−5835.
(107) Schäfer, A.; Horn, H.; Ahlrichs, R. Fully Optimized Contracted Gaussian Basis Sets for Atoms Lithium to Krypton. *J. Chem. Phys.* **1992**, *97*, 2571−2577.
(108) Neese, F. An Improvement of the Resolution of the Identity Approximation for the Calculation of the Coulomb Matrix. *J. Comput. Chem.* **2003**, *24*, 1740−1747.
(109) Chemcraft. graphical software for visualization of quantum chemistry computations., Version 1.8, build 682. https://www.chemcraftprog.com.
(110) Hirata, S.; Head-Gordon, M. Time-dependent Density Functional Theory within the Tamm−Dancoff Approximation. *Chem. Phys. Lett.* **1999**, *314*, 291−299.
(111) Hirata, S.; Head-Gordon, M. Time-dependent Density Functional Theory for Radicals: An Improved Description of Excited States with Substantial Double Excitation Character. *Chem. Phys. Lett.* **1999**, *302*, 375−382.
(112) Neese, F.; Petrenko, T.; Ganyushin, D.; Olbrich, G. Advanced aspects of ab initio theoretical optical spectroscopy of transition metal complexes: Multiplets, spin-orbit coupling and resonance Raman intensities. *Coord. Chem. Rev.* **2007**, *251*, 288−327.
(113) Angeli, C.; Cimiraglia, R.; Malrieu, J.-P. n-electron valence state perturbation theory: A spinless formulation and an efficient implementation of the strongly contracted and of the partially contracted variants. *J. Chem. Phys.* **2002**, *117*, 9138−9153.
(114) Angeli, C.; Cimiraglia, R.; Malrieu, J.-P. N-electron valence state perturbation theory: a fast implementation of the strongly contracted variant. *Chem. Phys. Lett.* **2001**, *350*, 297−305.
(115) Angeli, C.; Cimiraglia, R.; Evangelisti, S.; Leininger, T.; Malrieu, J.-P. Introduction of n-electron valence states for multi-reference perturbation theory. *J. Chem. Phys.* **2001**, *114*, 10252−10264.
(116) Schapiro, I.; Sivalingam, K.; Neese, F. Assessment of n-Electron Valence State Perturbation Theory for Vertical Excitation Energies. *J. Chem. Theory Comput.* **2013**, *9*, 3567−3580.

https://doi.org/10.1021/acs.organomet.5c00396
Organometallics XXXX, XXX, XXX−XXX